C. Teodosiu
J.L. Raphanel
F. Sidoroff
editors

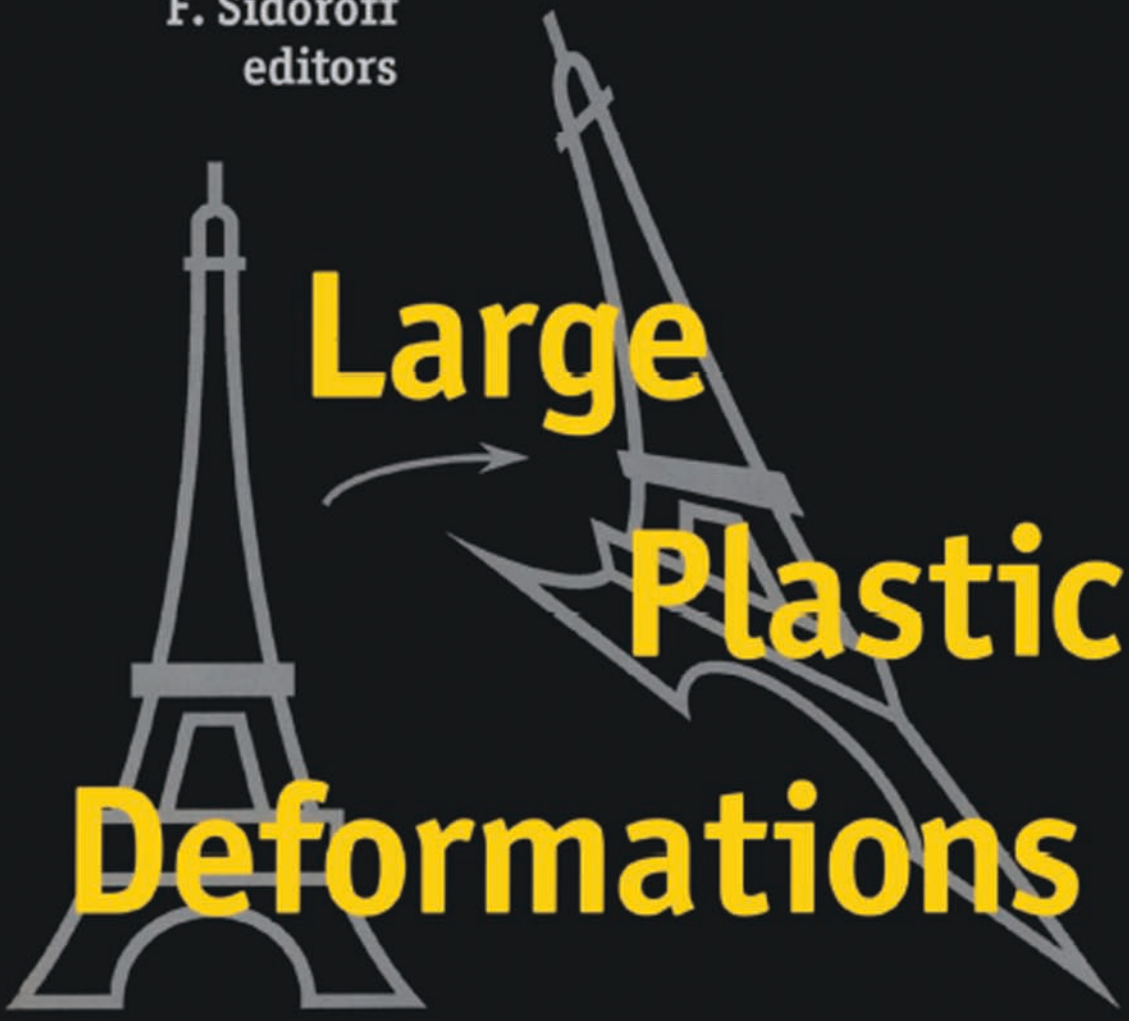

Large Plastic Deformations

Fundamental Aspects and Applications to Metal Forming

CRC Press
Taylor & Francis Group
A BALKEMA BOOK

LARGE PLASTIC DEFORMATIONS
FUNDAMENTAL ASPECTS AND APPLICATIONS TO METAL FORMING

PROCEEDINGS OF THE INTERNATIONAL SEMINAR MECAMAT'91
FONTAINEBLEAU / FRANCE / 7-9 AUGUST 1991

Large Plastic Deformations

Fundamental Aspects and Applications to Metal Forming

Edited by
C.TEODOSIU & J.L.RAPHANEL
LPMTM – CNRS, Université Paris Nord, Villetaneuse, France
F.SIDOROFF
LTDS, CNRS & Ecole Centrale de Lyon, France

CRC Press
Taylor & Francis Group
Boca Raton London New York

CRC Press is an imprint of the
Taylor & Francis Group, an **informa** business
A BALKEMA BOOK

Published by:
CRC Press/A. A. Balkema
P.O. Box 447, 2300 AK Leiden, The Netherlands
e-mail: Pub.NL@taylorandfrancis.com
www.crcpress.com – www.taylorandfrancis.com

CRC Press/Balkema is an imprint of the Taylor & Francis Group, an informa business

No claim to original U.S. Government works

ISBN 13: 978-90-5410-317-2 (hbk)

Visit the Taylor & Francis Web site at
http://www.taylorandfrancis.com

and the CRC Press Web site at
http//www.crcpress.com

The texts of the various papers in this volume were set individually by typists under the supervision of each of the authors concerned.

MECAMAT'91, Teodosiu, Raphanel & Sidoroff (eds) © 1993 Balkema, Rotterdam, ISBN 90 5410 317 5

Table of contents

Plastic heterogeneities and localization

MECAMAT'91, Teodosiu, Raphanel & Sidoroff (eds) © 1993 Balkema, Rotterdam, ISBN 90 5410 317 5

Preface

Since their inception in 1986, the goal of the MECAMAT International Seminars has been to promote a multidisciplinary approach in the Mechanics of Materials and to bring together scientists from the academic world and industry in order to address specific topics in this field from both a fundamental and an applied perspective. The previous seminars were held in France on the following themes: Local Approach of Fracture (Moret-sur-Loing, 1986), High Temperature Fracture and Mechanisms (Dourdan, 1987), Inelastic Behaviour of Solids, Models and Utilization (Besançon, 1988), Mechanics and Mechanisms of Damage in Composites and Multimaterials (Saint-Etienne, 1989).

The present seminar, which is the fifth in the series, has been jointly organized by MECAMAT (The French Group for the Mechanics of Materials) and LPMTM (Laboratoire des propriétés mécaniques et thermodynamiques des matériaux – CNRS, Université Paris Nord, Villetaneuse). It took place at Fontainebleau (France) from 7 to 9 August 1991 and covered topics involving the theory of large plastic deformations of metallic materials and its applications to metal forming.

In so far as large deformations are concerned, the following subjects have been addressed:

– *Single crystals and crystalline aggregates. Micro-macro transition*: hardening and flow rules for single crystals; modelling the plastic behaviour of multicrystals and crystalline aggregates; plastic spin.

– *Plastic heterogeneities and localization*: microstructural organization at large strains; shear banding; strain localization.

– *Constitutive modelling and model identification*: phenomenological and micromechanical models taking into account microstructure, texture and damage evolution; mechanical analysis of homogeneous and inhomogeneous tests; application to structural materials.

– *Modelling and simulation of metal forming*: modelling and simulation of cold and hot forming; experimental validation of the results.

The proceedings offer a genuine view on the synergism achieved by combining microstructural characterization and understanding, mechanical modelling and experiments, numerical analysis and computation.

The editors are grateful to all members of the International Scientific Committee for their help in reviewing and improving the manuscripts. They are particularly indebted to their colleagues B. Bacroix, M. Gaspérini and P. Gilormini for their significant contribution to the editing of these proceedings.

The Editors

MECAMAT'91, Teodosiu, Raphanel & Sidoroff (eds) © 1993 Balkema, Rotterdam, ISBN 90 5410 317 5

Organization

Co-Chairmen
C. Teodosiu & F. Sidoroff, France

International Scientific Committee
L. Anand, USA
A. Baltov, Bulgaria
S. Cescotto, Belgium
Y.F. Dafalias, USA/Greece
I. St. Doltsinis, Germany
Y. Estrin, Germany
J. Kratochvil, Czechoslovakia
E. Kröner, Germany
T. Leffers, Denmark
A. Molinari, France
Z. Mróz, Poland
K.W. Neale, Canada
A. Needleman, USA
M. Ortiz, USA
P. Perzyna, Poland
A.R.S. Ponter, UK
E. Soós, Romania
V. Tvergaard, Denmark
M. Tokuda, Japan
J.R. Willis, UK
A. Zaoui, France

Organizing Committee (France)
B. Bacroix
T. Bretheau
G. Cailletaud
O. Debordes
A. Dogui
M. Gaspérini
J.C. Gélin
P. Gilormini
A. Molinari
D. Nouailhas
J.L. Raphanel
F. Sidoroff
C. Teodosiu
A. Zaoui

Sponsors
Centre National de la Recherche Scientifique
Direction des Recherches et Etudes Techniques du Ministère de la Défense
Electricité de France
Ministère de la Recherche et de la Technologie
Pechiney
Renault
Université Paris Nord

Invited lectures

MECAMAT'91, Teodosiu, Raphanel & Sidoroff (eds) © 1993 Balkema, Rotterdam, ISBN 90 5410 317 5

Elasto-viscoplasticity: Constitutive modeling and deformation processing

L.Anand
Massachusetts Institute of Technology, Cambridge, Mass., USA

ABSTRACT: Recent progress in isotropic and anisotropic elasto-viscoplastic constitutive models for polycrystalline metals is reviewed, and the application of these constitutive models to some simple forming operations is described.

1 INTRODUCTION

The object of this paper is to briefly review some recent progress in constitutive modeling for deformation processing. The work reported here has been performed in collaboration with my (former and current) students Stuart Brown, Allen Lush, Gustavo Weber, Curt Bronkhorst, Antonios Zavaliangos, and Surya Kalidindi, as part of their doctoral dissertations. The publications on which this brief review is based are listed in the section on references. In writing this paper I will quote freely from the papers referenced, and keep references to the related work of others in the literature at a minimal level; an extensive bibliography may be found in the references cited.

The simplest, and most commonly used phenomenological theory for infinitesimal elastic-plastic deformations of polycrystalline metals at absolute temperatures less than approximately one-third the melting temperature of a material in degrees absolute, is the classical, rate-independent, flow theory with isotropic hardening. This classical model has been generalized to a finite-deformation, frame-indifferent form by Hill (e.g. 1967). For a recent review of this generalization see Hughes (1984). Some major limitations of this widely used finite-deformation constitutive model are:

1. The constitutive model is based on an additive decomposition of the stretching tensor into elastic and plastic parts, in which the elastic stretching is related to the Jaumann derivative of the stress. In the abscence of plastic flow, this leads to a *hypoelastic* relation for the stress. Although the hypoelastic form of the constitutive equation for stress is a good approximation for metals under situations where elastic strains remain small, as has long been recognized, in the absence of plastic flow hypoelastic equations for stress lead to dissipation in closed cycles of deformation.
2. The notion of rate-independence of plastic response is only a convenient approximation at low homologous temperatures. Even at low temperatures, plastic flow due to dislocation motion is inherently rate-dependent.
3. Although the "finite deformation" constitutive model is formulated within a rigorous kinematical framework, it is in essence an extension of the classical small strain "isotropic hardening" plasticity model, and is accordingly expected to be useful for describing the deformation behavior of initially isotropic materials up to deformation levels where significant anisotropy of the metal has not developed.

In what follows we review our recent work on constitutive equations for polycrystalline metallic materials which overcome these shortcomings.

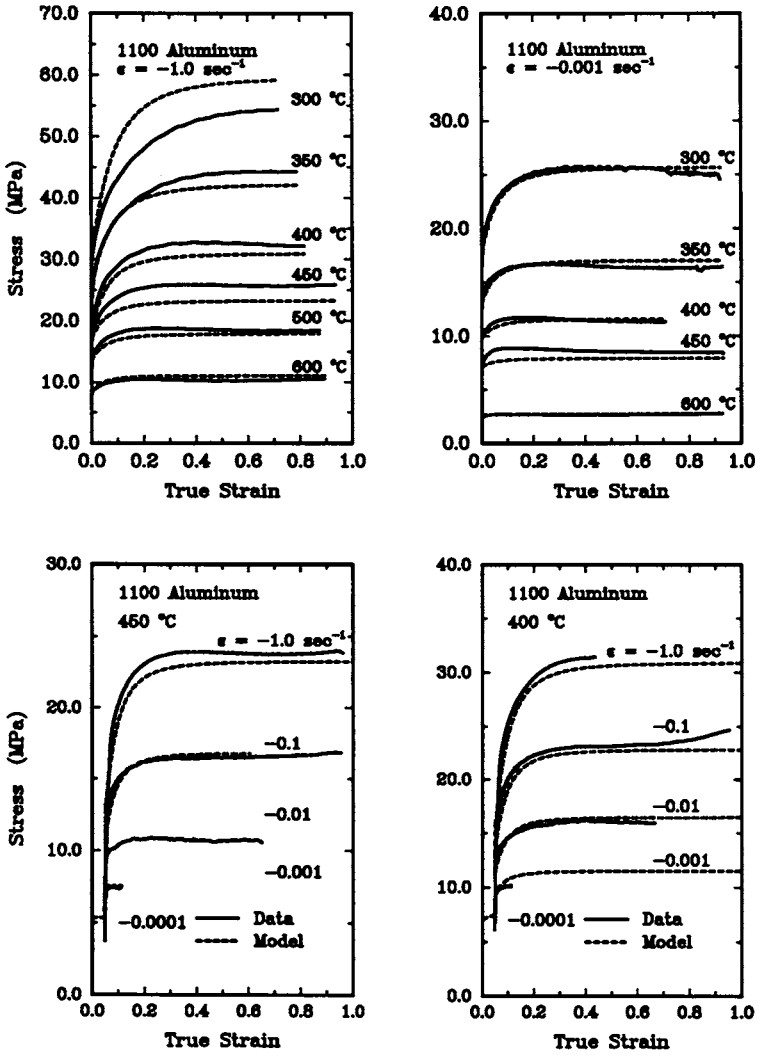

Fig.1 Correlation of the constitutive model with isothermal constant true strain rate and strain rate jump experiments

We will consider elastic-plastic constitutive models with *hyperelastic* relations for the stress. The plastic part of our constitutive models will be based on the following physical ideas:

- Plastic deformation due to dislocation motion is inherently rate-dependent.
- The instantaneous response of a material is determined by its current state. The current state (which is produced by the entire past history of deformation undergone by the material) may be assumed to be representable by a small number of macroscopic *internal variables*, and their evolution to be representable by rate equations.

In particular we shall consider two constitutive models:

1. A simple isotropic model for deformations at high homologous temperatures. This model neglects the inherently anisotropic nature of metals, and employs (just as in

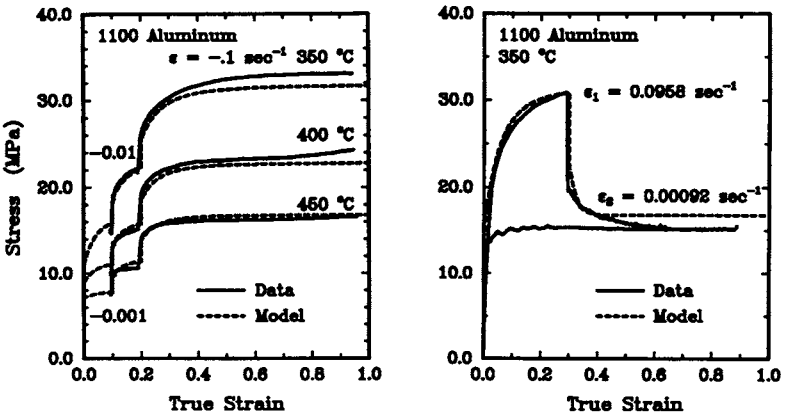

Fig.2 Predicted and actual stress response for (a) double jump experiments and (b) strain rate decrement experiment

the classical rate-independent, isotropic hardening theory) a single scalar internal variable to model an "isotropic" deformation resistance offered by the material. This constitutive model is expected to be valid only for initially isotropic materials subjected to deformation levels where significant texturing has not developed.

2. A simple anisotropic polycrystal model for deformations at low homologous temperatures. This model accounts for the polycrystalline nature of metals and accounts for the dominant mechanism of inelastic deformation by crystallographic slip at these temperatures. The internal variables in this model are the orientations of the slip systems, and the slip system deformation resistances.

These elasto-viscoplastic constitutive models for (1) the isotropic idealization of inherently anisotropic polycrystalline materials, and (2) anisotropic response, represent significant improvements over constitutive models currently used to simulate forming operations.

We use the following notation: $\mathbf{F}$, deformation gradient; $\mathbf{L}$, velocity gradient; $\mathbf{D}$, stretching; $\mathbf{W}$, spin; $\mathbf{T}$, Cauchy stress; θ, absolute temperature.

2 ISOTROPIC MODEL

The simplest, and most commonly used phenomenological model for infinitesimal elastic-plastic deformations is the classical J_2 flow theory with isotropic hardening. The set of constitutive equations for isotropic elastic-viscoplastic solids considered here (excerpted from papers by Anand, 1979, 1982, 1985, 1986) is essentially a generalization of this widely used theory to model *finite elastic and plastic* deformations, and rate-dependence of plastic flow. This set of constitutive equations consists of:

- The constitutive equation for stress:

$$\mathbf{T}^* = \mathcal{L}\,[\mathbf{E}^*] - \mathbf{\Pi}\,(\theta - \theta_0)\,, \tag{1}$$

$$\mathbf{E}^* \equiv \ln \mathbf{U}^*, \quad \mathbf{T}^* \equiv \mathbf{R}^{*T}\,\{(\det \mathbf{U}^*)\,\mathbf{T}\}\,\mathbf{R}^*, \tag{2}$$

$$\mathcal{L} \equiv 2\mu\mathcal{I} + (\kappa - (2/3)\mu)\,\mathbf{1}\otimes\mathbf{1}, \quad \mathbf{\Pi} \equiv 3\,\kappa\,\alpha\,\mathbf{1}, \tag{3}$$

where $\mathbf{E}^*$ is the logarithmic elastic strain, $\mathbf{T}^*$ is the stress measure which is elastic work conjugate to this strain measure, $\mathcal{L}$ is the fourth order isotropic elasticity tensor, with $\mu = \hat{\mu}(\theta)$ and $\kappa = \hat{\kappa}(\theta)$ elastic shear and bulk moduli, respectively, $\alpha = \hat{\alpha}(\theta)$ is the coefficient of thermal expansion, $\mathcal{I}$ the fourth order symmetric identity tensor, $\mathbf{1}$ is the second order identity tensor, and θ_0 is a reference temperature. Also, $\mathbf{U}^*$ and $\mathbf{R}^*$ are the elastic right stretch and elastic rotation tensors, respectively, in the polar decomposition

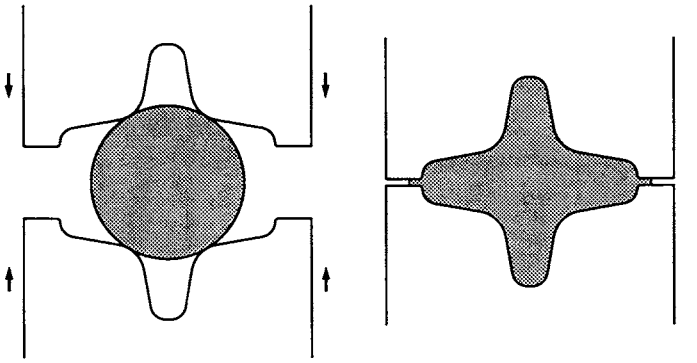

Fig.3 Schematic of the plane-strain forging process converting a billet from a circular to a cruciform cross-section

of an elastic deformation gradient $\mathbf{F}^*$. The elastic deformation gradient is defined in terms of the total deformation gradient $\mathbf{F}$ and a plastic deformation gradient $\mathbf{F}^p$, with $\det \mathbf{F}^p = 1$, by

$$\mathbf{F}^* \equiv \mathbf{F}\mathbf{F}^{p-1}, \qquad \det \mathbf{F}^* > 0. \tag{4}$$

The plastic deformation gradient is in turn given by the flow rule prescribed below.

- The evolution equation for $\mathbf{F}^p$ — the "flow rule":

$$\dot{\mathbf{F}}^p = \mathbf{L}^p \mathbf{F}^p, \tag{5}$$

with

$$\mathbf{D}^p \equiv \operatorname{sym} \mathbf{L}^p = \hat{\mathbf{D}}^p(\mathbf{T}^*, \theta, \bar{s}) = \sqrt{3/2}\, \dot{\bar{\epsilon}}^p\, \mathbf{N}, \tag{6}$$

and

$$\mathbf{W}^p \equiv \operatorname{skw} \mathbf{L}^p = \mathbf{0}, \tag{7}$$

where $\mathbf{N} = \sqrt{3/2}\, (\mathbf{T}^{*\prime}/\bar{\sigma})$ is the direction of plastic stretching, $\mathbf{T}^{*\prime}$ is the deviator of $\mathbf{T}^*$, $\bar{\sigma} \equiv \sqrt{(3/2)\mathbf{T}^{*\prime} \cdot \mathbf{T}^{*\prime}}$ is the equivalent tensile stress, and

$$\dot{\bar{\epsilon}}^p = f(\bar{\sigma}, \theta, \bar{s}) \tag{8}$$

is an equivalent tensile plastic strain rate.

The variable $\bar{s}$ is an internal state variable which is taken to have the dimensions of stress, and is called the *deformation resistance*. It evolves according to its evolution equation given below.

- Evolution equation for the deformation resistance $\bar{s}$:

$$\dot{\bar{s}} = h\dot{\bar{\epsilon}}^p - \dot{r}, \quad h = \hat{h}(\bar{\sigma}, \theta, \bar{s}), \quad \dot{r} = \hat{\dot{r}}(\theta, \bar{s}), \tag{9}$$

where $\hat{h}$ is a hardening and dynamic recovery function, and $\hat{\dot{r}}$ is a static recovery function.

For the plastic part of these constitutive equations we note that there is a departure from the classical theories — no yield conditions and attendant loading/unloading criteria are assumed. The model belongs to the so-called class of 'unified constitutive equations' in which 'plasticity' and 'creep' are unified, in that they are described by the same set of flow and evolutionary equations. The overall mathematical structure of this rate dependent plasticity model is simple because the plastic flow rule is a smooth function, although the particular form of the constitutive function for $\dot{\bar{\epsilon}}^p$ may be mathematically very stiff in certain regions of plastic flow, requiring special care in formulating numerical algorithms.

To complete this rate-dependent constitutive model for a particular material the material properties/functions that need to be specified are the elastic shear and and bulk moduli, μ and κ, respectively, the flow function for the equivalent tensile plastic strain rate in (8), and the evolution function for the deformation resistance in (9).

Based on their hot compression experiments on an iron-2% silicon alloy and a commercially pure aluminum (performed in the homologous temperature range 0.6 to 0.9 and the strain rate range 10^{-3} to 10^{0} sec^{-1}), Brown, Kim and Anand (1989) have proposed the following specific constitutive functions for $\dot{\bar{\epsilon}}^p$ and $\dot{\bar{s}}$:

$$\dot{\bar{\epsilon}}^p = A \exp\left(-\frac{Q}{R\theta}\right) \left[\sinh\left(\xi \frac{\bar{\sigma}}{\bar{s}}\right)\right]^{1/m}, \tag{10}$$

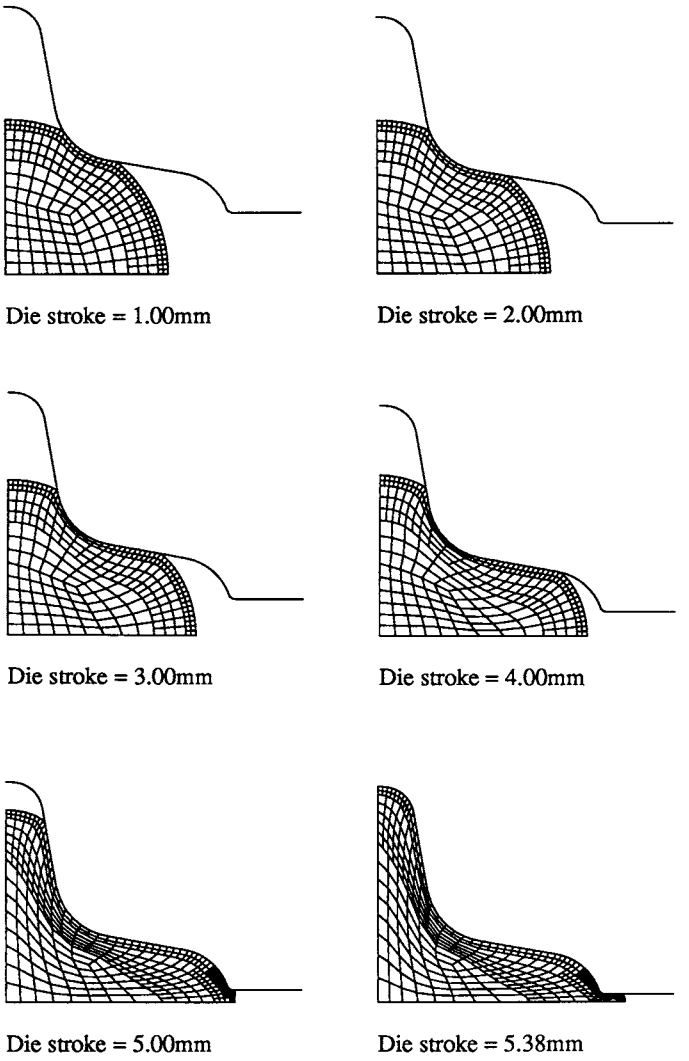

Fig.4 Finite element meshes at several stages of deformation
The model has been remeshed when necessary

$$\dot{\bar{s}} = \left\{ h_0 \left| \left(1 - \frac{\bar{s}}{s^*}\right) \right|^a \operatorname{sign}\left(1 - \frac{\bar{s}}{s^*}\right) \right\} \dot{\bar{\epsilon}}^p, \quad (11)$$

with

$$s^* = \hat{s} \left[\frac{\dot{\bar{\epsilon}}^p}{A} \exp\left(\frac{Q}{R\theta}\right) \right]^n . \quad (12)$$

The list of material parameters in these constitutive equations are: A, Q, m, ξ, $h_0, a, \hat{s}$, and n. Also R is the universal gas constant. In their paper Brown *et. al* detail a systematic procedure used to determine these material parameters from appropriate experimental data. For 1100-O they find $A = 1.91 \times 10^7\,\mathrm{sec}^{-1}$, $Q = 175.3$ kJ/mole, $m = 0.23$, $\xi = 7.0$, $h_0 = 1115.6$ MPa, $a = 1.3$, $\hat{s} = 18.9$ MPa, and $n = 0.07$. In their paper they also list values of s_0 and the elastic moduli as a function of temperature.

Fig. 1 shows that for this material the constitutive model reasonably well duplicates the physical data upon which the model is based and from which the material parameters of the model have been determined. This figure presents representative simulations of isothermal, constant true strain rate and strain rate jump experiments,

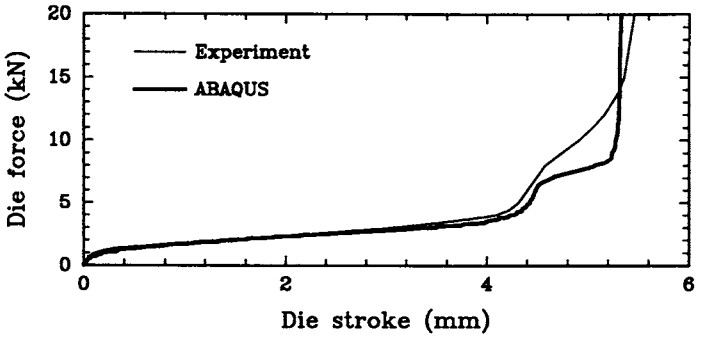

Fig. 5 Die force versus die stroke for plane-strain forging example.

together with the original experimental data. The correlation between the model and the experimental data is very good.

Amongst the various experiments performed by Brown, Kim and Anand (1989) to test the predictive capability of the constitutive model are experiments in which the strain rate is suddenly increased twice, and other experiments in which there is a sudden decrease in the strain rate. Fig. 2a shows the results from experiments where the strain rate is rapidly increased twice. The model reproduces the double jump test data very well, duplicating both the instantaneous, constant structure strain rate dependence, and the subsequent strain hardening. Fig. 2b. shows experimental results and the corresponding numerical simulation of a strain rate decrement test. This test shows the predictive capability of the model to handle strain softening. The steady state stress reached after the strain rate decrement corresponds to the steady state value for a monotonic test at the final strain rate and temperature, and this is well predicted by the constitutive model.

The constitutive model accounts for the physical phenomena of strain rate and temperature sensitivity, strain rate history effects, strain hardening and the restoration process of dynamic recovery. As compared to the currently used constitutive models which take the equivalent plastic strain rate to be a simple power-law or a hyperbolic sine function of the equivalent stress, together with a temperature dependence of an Arrhenius form, and which do not account for any internal structural evolution, the constitutive model presented above is a major improvement.

Weber and Anand (1990) have formulated a stable time integration procedure for the *isothermal* version of this constitutive model. The time-integration procedure has been implemented in the finite element program ABAQUS (1990) by writing a "user material" subroutine. Using this computer code representative hot, isothermal, forging problems have been solved. As an example we present a plane strain forging which has also been considered by Lush, Weber and Anand (1989). The constitutive model used by Lush *et al.* is similar in all respects to the one considered here, except that for the elasticity they use a hypoelastic formulation, instead of the hyperelastic formulation used here.

A miniature, hot, isothermal, closed die forging test has been performed on aluminum 1100-O for the purpose of comparing the predictions of constitutive equations and computational procedures against experimental results from an actual forging operation. The plane-strain forging process converts the cross section of a cylindrical aluminum billet from a circular to a cruciform shape, as shown in Figure 3. Proper sizing of the billet ensures that the dies would be filled, and that a small amount of flash would be produced. An oil-based graphite lubricant had been applied to the die and billet surfaces to minimize the effects of friction. The temperature of the billet and dies was maintained at 400°C. Isothermal conditions were approximated by loading at a slow rate of 0.1 mm/sec. This forging example exhibits many important features such as: (1) nonhomogeneous deformation, (2) variable regions of contact between billet and dies, (3) time-varying deformation rates at material points, and (4) rapid rise of total die

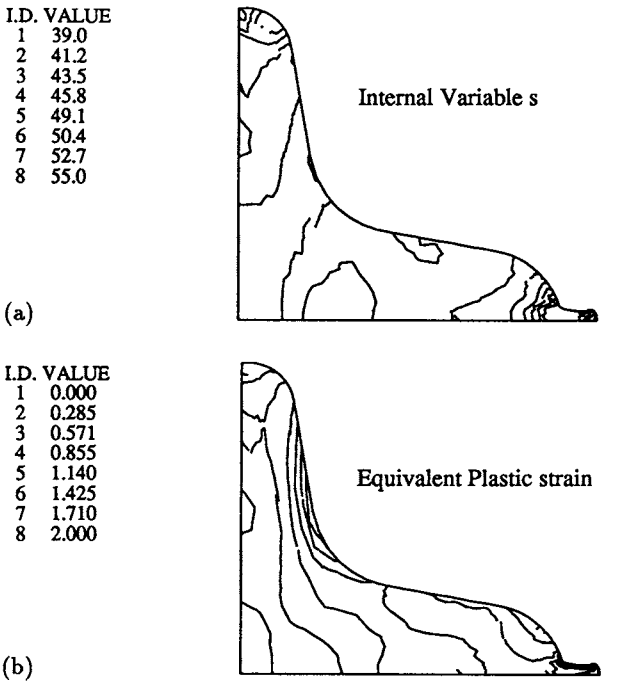

Fig. 6 Contours of internal variable $\bar{s}$ and equivalent plastic strain after 5.38 mm die stroke in the plane-strain forging example.

force when the dies became filled.

In the finite element analysis it was assumed that there were two planes of symmetry in the specimen and dies[1]. Accordingly, only one quadrant of the specimen was modeled, and contact in the finite element calculations was modeled as frictionless.

Figure 4 shows the finite element mesh after several stages of deformation. A remeshing scheme was used to rectify any deterioration of mesh quality in this large deformation problem. Until around 4 mm of stroke, the material flow is seen to be predominantly horizontal. When the die becomes filled in this direction, the flow pattern changes and the load is seen to rise in Figure 5. Horizontal die filling occurred at a slightly smaller die stroke in the experiment than in the finite element calculation, but this can be attributed to slight imperfections in the die shape and asymmetry in the flow, which were not modeled. Frictional effects associated with breakdown of the lubricant layer as a result of large sliding motions may also have contributed to the discrepancy between the calculated and measured die force versus stroke curves. Contours of internal variable $\bar{s}$ after 5.38 mm die stroke are shown in Figure 6(a). Contours of equivalent plastic tensile strain after 5.38 mm die stroke are shown in Figure 6(b).

The major new features of this work on isotropic elasto-viscoplasticity and the associated computational procedures are that:

1. The constitutive equations for the plastic part of the model are a natural, more physical generalization of the classical J_2, rate-independent flow theory. Indeed, special forms of the viscoplastic constitutive functions have been shown by Brown, Kim and Anand (1989) to be in good agreement with experiments for large deformations at high temperatures.

2. In the absence of plastic flow the constitu-

[1]This was not quite representative of the actual experiments since there was some asymmetry in the dies used in the physical forging experiments. This causes some of the discrepancy between the experimental die force versus die stroke results and the corresponding numerical simulations observed in Fig. 5

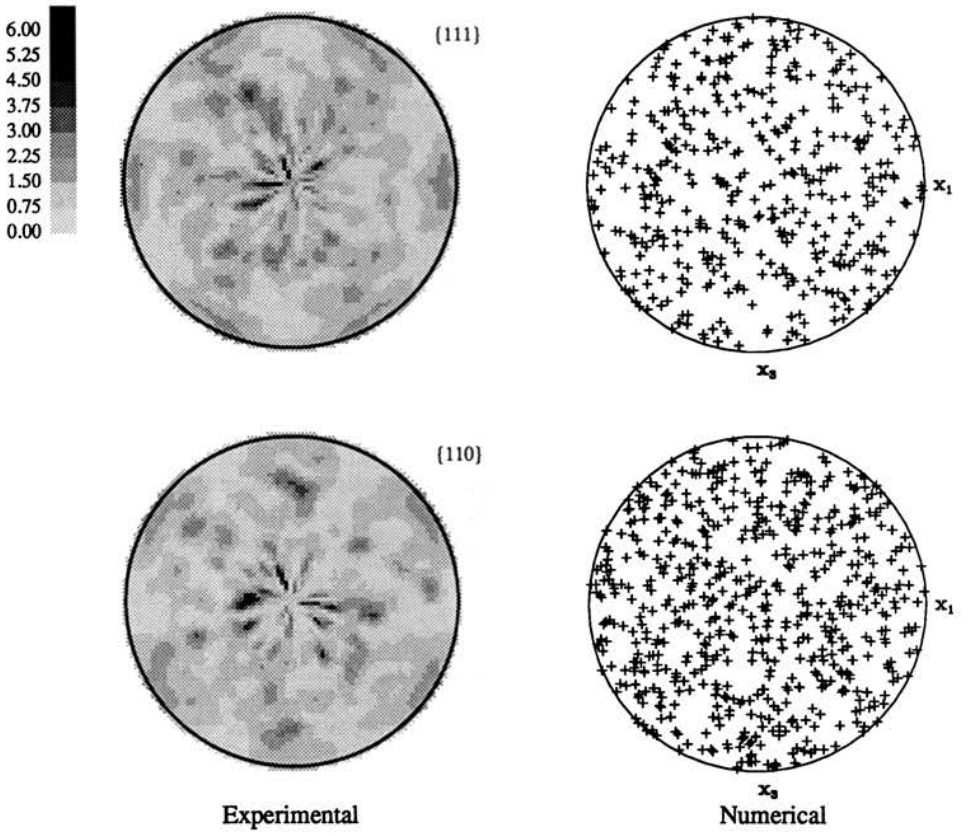

Fig. 7. Experimental measurement of the initial texture for annealed copper and its numerical representation using one hundred grains. The pole figures shown are the equal-area projections of the specified crystallographic planes.

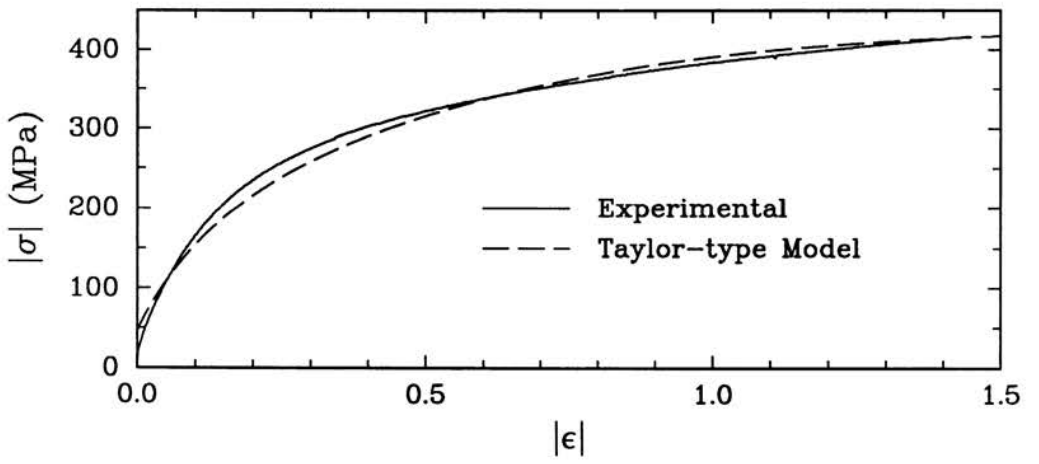

Fig. 8. Experimentally measured axial stress versus logarithmic axial strain response in simple compression and its representation by a Taylor-type anisotropic plasticity model.

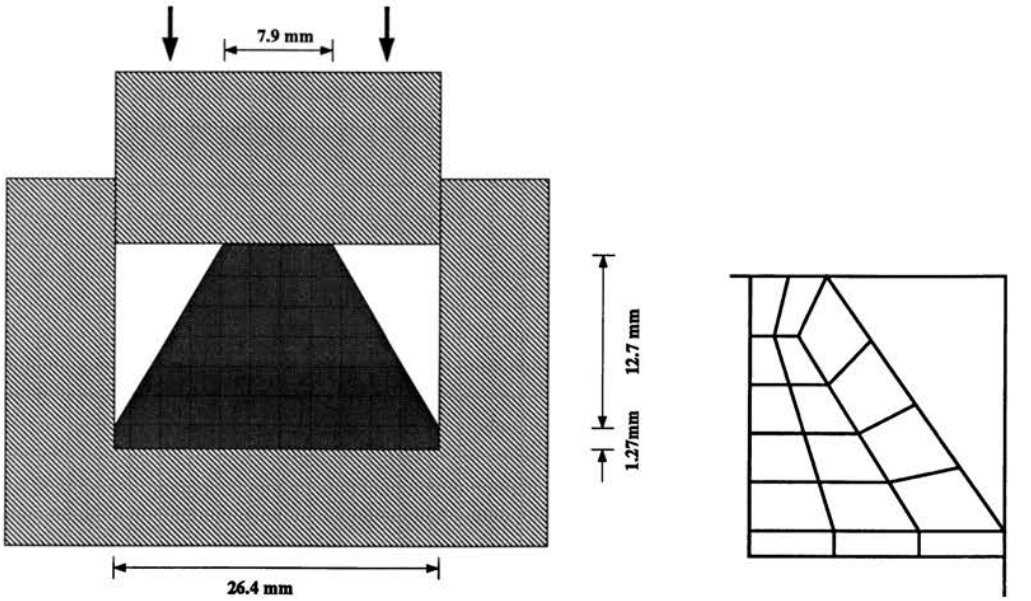

Fig. 9. (a) Schematic of a plane strain block forging experiment. (b) Coarse mesh used for finite element simulation.

tive equations reduce to a hyperelastic relation which has also been previously shown by Anand (1979, 1986) to be in good agreement with experiments for moderately large elastic deformations.

3. The time integration procedure of Weber and Anand (1990) is a generalization of the classical radial-return algorithm. It is implicit, robustly stable, and "numerically objective".

These features of this work make it well suited for large scale computations for simulation of hot-working processes. The obvious limitation of this constitutive model is that it does not account for the evolving anisotropy associated with large plastic deformations. To rectify this situation we consider next an anisotropic polycrystalline plasticity model.

3 ANISOTROPIC MODEL.

In polycrystalline metals the major cause of anisotropic plastic response is crystallographic texture resulting from the reorientation of the crystal lattices of grains during deformation. There have been considerable recent advances in the understanding of anisotropy due to crystallographic texturing. Asaro and Needleman (1985) have developed an elastic-plastic, rate-dependent polycrystalline model for low homologous temperatures in which plastic deformation within the individual crystals is taken to be by crystallographic slip alone. To predict the global response of the polycrystal, the transition from the micro-response of the individual grains to the macro-response of the polycrystalline aggregate, Asaro and Needleman follow the pioneering work of Taylor (1938) and assume that all grains have equal volume, and that the deformation gradient within each grain has a uniform value throughout the aggregate. In this approximate model, compatibility is satisfied and equilibrium holds in each grain, but equilibrium is usually violated between grains. This simple averaging procedure gives that the macroscopic average Cauchy stress in the polycrystal is simply the number average of the Cauchy stress in each crystal. In this model, the deformation producing mechanisms of twinning, diffusion and grain boundary

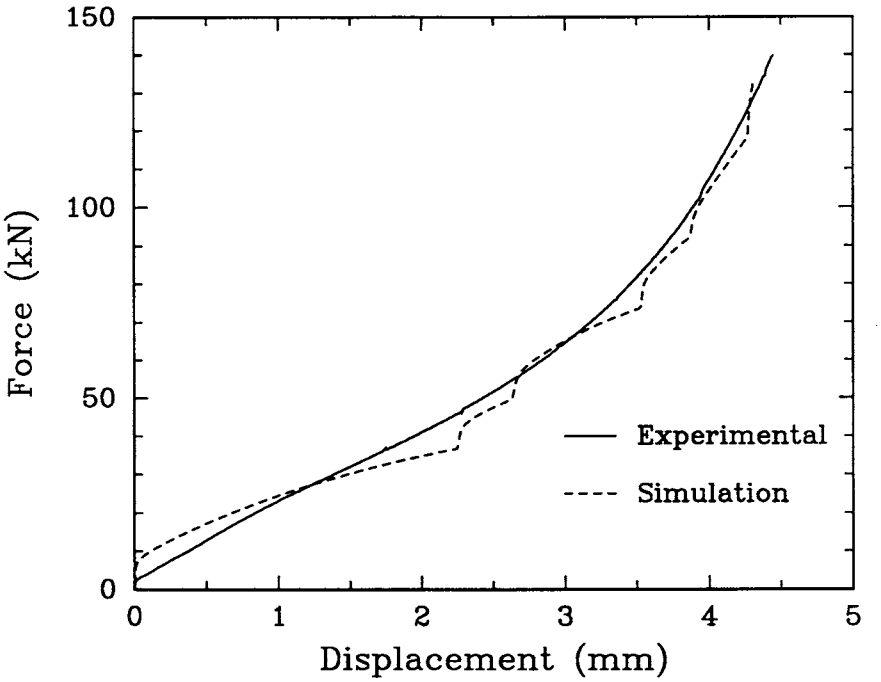

Fig. 10. Experimental and predicted load-displacement curves for the block forging experiment.

sliding are not considered, and other sources of anisotropy due to the morphological effects of grain shape, size and arrangement are not taken into account.

In what follows, we give a brief description of a slightly modified form of the generalized Taylor-type polycrystal constitutive model of Asaro and Needleman (1985). We confine our attention to infitesimal elastic strains, low homologous temperatures and isothermal conditions.

The stress response at each macroscopic continuum material point is taken to be given by the volume averaged response of the multitude of microscopic single crystalline grains comprising the material point. The essential assumptions in the Taylor-type polycrystal model are that all grains have equal volume, and that the local deformation gradient in each grain is homogeneous and identical to the macroscopic deformation gradient $\mathbf{F}$ at the continuum material point level. Then, with $\mathbf{T}^{(k)}$ denoting the Cauchy stress in the k^{th} crystal, these assumptions lead to:

$$\bar{\mathbf{T}} = \frac{1}{N} \sum_{k=1}^{N} \mathbf{T}^{(k)}, \tag{13}$$

where $\bar{\mathbf{T}}$ is the volume averaged stress, and N is the total number of grains comprising the material point.

The constitutive equation for the stress *in each grain* is taken as

$$\mathbf{T}^* = \mathcal{L}[\mathbf{E}^*], \tag{14}$$

with $\mathbf{E}^* = (1/2)\left\{\mathbf{F}^{*T}\,\mathbf{F}^* - \mathbf{1}\right\}$ and $\mathbf{T}^* = \mathbf{F}^{*-1}\,\{(\det\mathbf{F}^*)\,\mathbf{T}\}\,\mathbf{F}^{*-T}$ denoting work conjugate elastic strain and stress measures[2], respectively, and $\mathcal{L}$ is a fourth order elasticity tensor. Also, $\mathbf{T}$ is the symmetric Cauchy stress tensor in the grain, and $\mathbf{F}^*$ is a local elastic deformation gradient defined in terms of the local deformation gradient $\mathbf{F}$ (equal to the macroscopic deformation gradient by virtue of the Taylor assumption) and a local plastic deformation gradient $\mathbf{F}^p$, with $\det\mathbf{F}^p = 1$ (plastic incompressibility), by $\mathbf{F}^* \equiv \mathbf{F}\mathbf{F}^{p-1}$, $\det\mathbf{F}^* > 0$.

The plastic deformation gradient is in turn given by the flow rule

[2]For infinitesimal elastic strains the choice of work conjugate strain and stress pairs is not significant.

$$\dot{\mathbf{F}}^p = \mathbf{L}^p \mathbf{F}^p, \tag{15}$$

with

$$\mathbf{L}^p = \sum_\alpha \dot{\gamma}^\alpha \mathbf{S}_o^\alpha, \qquad \mathbf{S}_o^\alpha \equiv \mathbf{m}_o^\alpha \otimes \mathbf{n}_o^\alpha, \tag{16}$$

and

$$\dot{\gamma}^\alpha = \hat{\dot{\gamma}}^\alpha (\tau^\alpha, s^\alpha), \qquad \tau^\alpha \equiv \mathbf{T}^* \cdot \mathbf{S}_o^\alpha. \tag{17}$$

Here, $\mathbf{m}_o^\alpha$ and $\mathbf{n}_o^\alpha$ are *time-independent* orthonormal unit vectors which define the slip direction and slip plane normal of the slip system α in a fixed reference configuration. The quantity $\dot{\gamma}^\alpha$ is the plastic shearing rate on the slip system α, and is taken to be given in terms of a resolved shear stress τ^α and a slip system deformation resistance s^α.

The slip resistance s^α is taken to evolve as

$$\dot{s}^\alpha = \sum_\beta h^{\alpha\beta} \left| \dot{\gamma}^\beta \right|, \tag{18}$$

where $h^{\alpha\beta}$ is the rate of strain hardening on slip system α due to a shearing on the slip system β.

For fcc metals the elastic anisotropy of the fcc single crystals is not strong, and the elasticity tensor $\mathcal{L}$ may be approximated by

$$\mathcal{L} \equiv 2\mu \mathcal{I} + (\kappa - (2/3)\mu)\, \mathbf{1} \otimes \mathbf{1}, \tag{19}$$

where μ and κ are the elastic shear and bulk moduli, respectively. The specific constitutive functions for the plastic shearing rate $\dot{\gamma}^\alpha$ on a slip system and the hardening matrix $h^{\alpha\beta}$ are taken as:

$$\dot{\gamma}^\alpha = \dot{\gamma}_o \left| \frac{\tau^\alpha}{s^\alpha} \right|^{1/m} \operatorname{sign}(\tau^\alpha), \tag{20}$$

where $\dot{\gamma}_o$ and m are material parameters representing a reference shearing rate and the rate sensitivity of slip, and

$$h^{\alpha\beta} = q^{\alpha\beta} h^{(\beta)} \qquad (\text{no sum on } \beta), \tag{21}$$

where $h^{(\beta)}$ is a single slip hardening rate and $q^{\alpha\beta}$ is a matrix describing the latent hardening behavior of a crystallite. Following Asaro and Needleman (1985), for the twelve $\{111\} < 110 >$ type slip systems for fcc crystals, we take $q^{\alpha\beta}$ to be given by

$$q^{\alpha\beta} = \begin{Bmatrix} A & qA & qA & qA \\ qA & A & qA & qA \\ qA & qA & A & qA \\ qA & qA & qA & A \end{Bmatrix}, \tag{22}$$

where q is the ratio of the latent hardening rate to the self hardening rate, and A is a 3×3 matrix fully populated by ones. In equation 22, systems $\{1,2,3\}$ are coplanar, as are systems $\{4,5,6\}$, $\{7,8,9\}$, and $\{10,11,12\}$. Thus the ratio of the latent hardening rate to the self hardening rate for coplanar slip systems is unity.

Finally, motivated by the work of Brown, Kim and Anand (1989), we adopt the following specific form for the single slip hardening rate in equation 21:

$$h^{(\beta)} = h_o \left\{ 1 - \frac{s^\beta}{s_s} \right\}^a, \tag{23}$$

where h_o, a, and s_s are slip system hardening parameters which are taken to be identical for all slip systems. In this saturation form of the single slip hardening rate, we take the saturation value s_s to be a constant. This saturation value should in general be an increasing function of the strain rate; this would account for a rate sensitivity of the rate of strain hardening (see Section 2), but at low homologous temperatures this is a second order effect.

In a recent paper (Kalidindi, Bronkhorst and Anand, 1991), we have developed a new *implicit* time-integration procedure for this generalized Taylor-type polycrystal constitutive model. We have implemented the polycrystal constitutive model, together with our time-integration procedure, in the finite element program ABAQUS (1990). Our constitutive model and computational procedures can be used in finite element calculations where an integration point represents a material point in a polycrystalline sample and the constitutive response at the integration point is given through the Taylor-type polycrystal model. Using these mathematical tools, we have demonstrated the predictive capabilities of the Taylor-type constitutive model and our computational procedures for bulk deformation processing by comparing predictions of the overall load-displacement response and the evolution of crystallographic texture against corresponding experimental results from a simple, non-homogeneous, plane-strain forging experiment.

The forging experiment was performed on

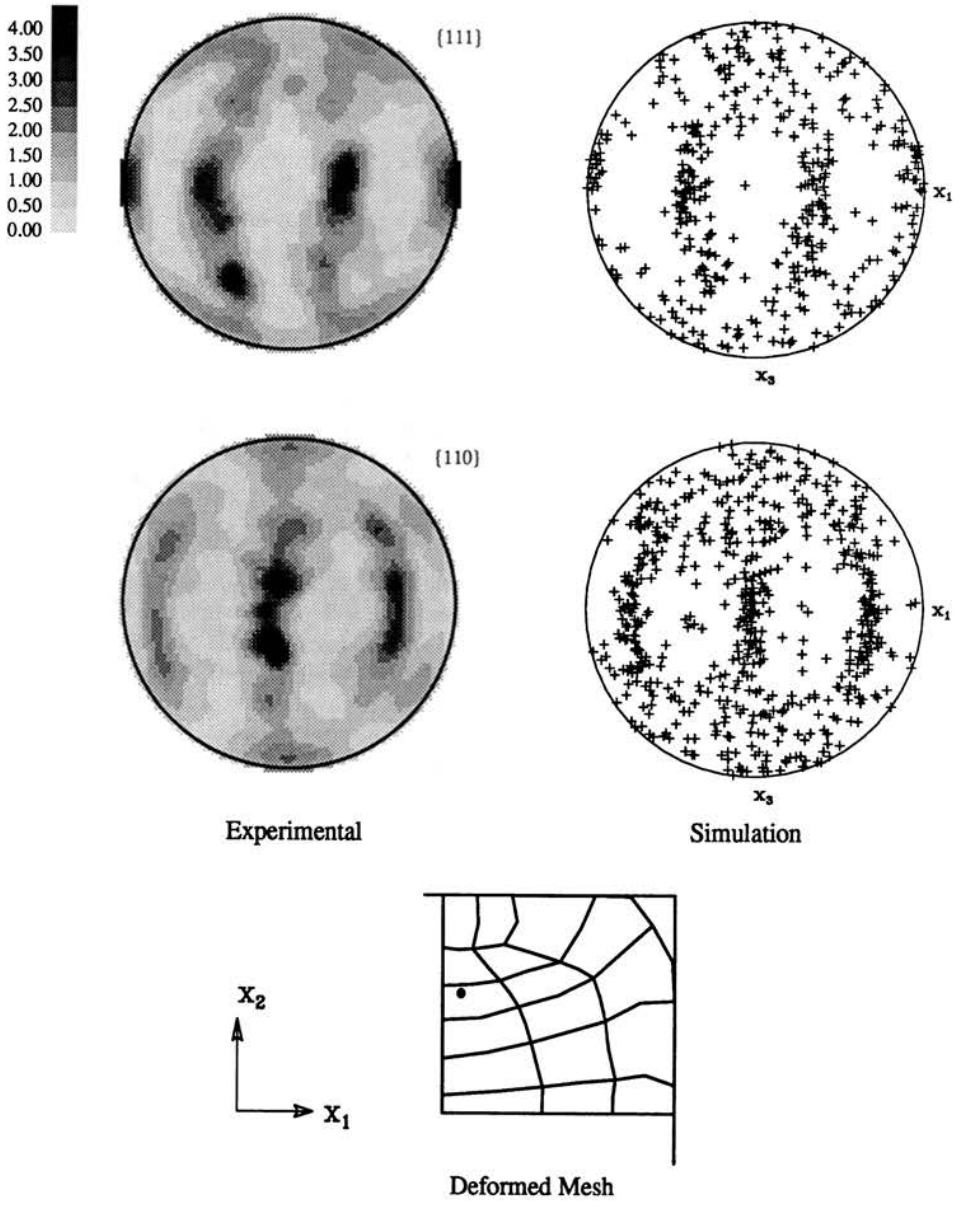

Fig. 11. (a) {111} and {110} (equal-area projection) experimental pole figures from the deformed specimen and the corresponding simulation at the point indicated in the deformed mesh.

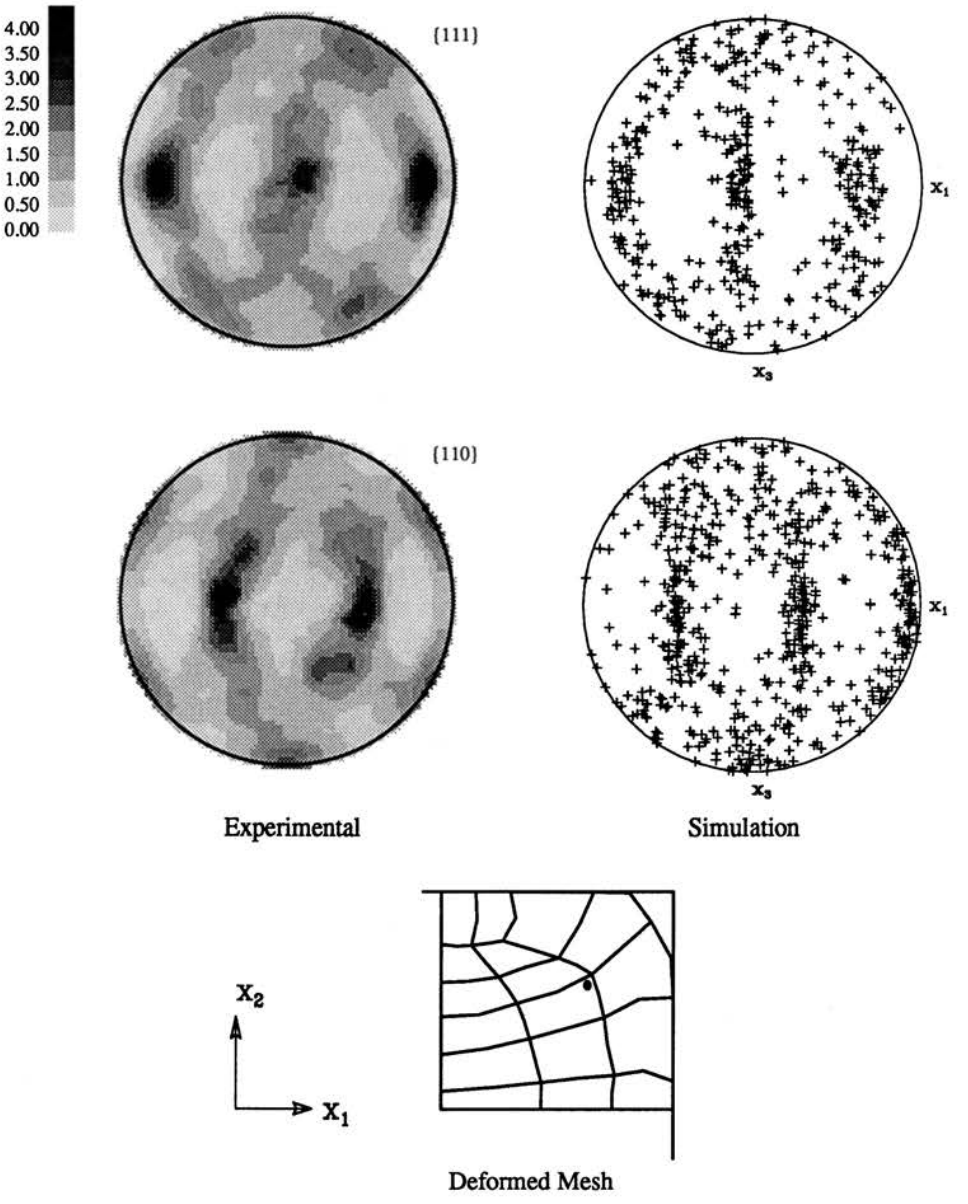

Fig. 11. (b) {111} and {110} (equal-area projection) experimental pole figures from the deformed specimen and the corresponding simulation at the point indicated in the deformed mesh.

annealed[3] OFHC copper. This material was assumed to have an "isotropic" initial texture, and this texture for simulating the inhomogeneous forging experiment was represented by 100 crystals at each integration point whose orientations are given by Molinari, Canova and Ahzi (1987). Fig. 7 shows a comparison of the { 111} and {110} (equal-area projection) pole figures[4] corresponding to the assumed initial set of crystal orientations and actual texture measurements from an annealed specimen.

The values of the material parameters used in the calculations by Kalidindi, Bronkhorst and Anand (1991) are[5] $\mu = 46.5\,\text{GPa}$, $\kappa = 124$ GPa, $\dot{\gamma}_o = 0.001\,\text{s}^{-1}$, $m = 0.012$, $q = 1.4$, $h_o = 180\,\text{MPa}$, $a = 2.25$, and $s_s = 148\,\text{MPa}$, together with an initial value of the slip system deformation resistance of $s_o = 16\,\text{MPa}$. The correspondence between the stress-strain results from a simulation of a simple compression experiment using these material parameters in the Taylor-type polycrystal model, and the experimental data (from which the material parameters were determined) is shown in Fig. 8. The agreement is reasonable.

A schematic of the forging is shown in Fig. 9a. Using the coarse mesh shown in Fig. 9b, a computer simulation was performed to predict the load-displacement curve and the evolved textures at several points in the specimen. The predicted and experimental load-displacement curves are shown in Fig. 10, while the evolved textures at two representative points in the sample are shown in Figs. 11a and 11b. These figures show a good first order agreement between the predictions and experimental results.

4 CONCLUSIONS

To the best of our knowledge, the paper by Kalidindi, Bronkhorst and Anand (1991) is the first report of a simulation and corresponding comparison against experiments of the evolution of crystallographic texture in a non-homogeneous, non-steady deformation processing operation. However, this finite element simulation of a very simple forging, and which used a *coarse* mesh containing only seventeen elements, took about 150 CPU hours on a SUN 4/330 workstation. Clearly, calculation procedures which exploit substantial vectorization and parallelization of the computational procedures reported in Kalidindi *et al.*, and which also take into account new computer architectures, are necessary to expand the scope of polycrystalline plasticity calculations for predicting the evolution of crystallographic texture to realistic deformation processing operations. Meanwhile, the isotropic plasticity model reviewed in this paper offers substantial improvements over currently used plasticity models used to simulate, analyse and design forming operations.

ACKNOWLEDGEMENT

The support of the Solid Mechanics Program of the U.S. Office of Naval Research under grant (ONR No. 0014-89-J-3040) and the Materials Processing and Manufacturing Program of the U.S. National Science Foundation (DDM-8914161) is gratefully acknowledged.

REFERENCES

ABAQUS Reference Manuals,1990, Hibbitt, Karlsson and Sorensen Inc., Providence R.I.

Anand, L., 1979. On H. Hencky's Approximate Strain Energy Function for Moderate Deformations. *ASME Journal of Applied Mechanics* 46: 78-82.

Anand, L., 1982. Constitutive Equations for the Rate-Dependent Deformation of Metals at Elevated Temperatures. *ASME Journal of Engineering Materials and Technology* 104: 12-17.

Anand, L., 1985. Constitutive Equations for Hot Working of Metals. *International Journal of Plasticity* 1: 213-231.

Anand, L.,1986. Moderate Deformations In Extension Torsion of Incompressible Isotropic Elastic Materials. *Journal of the Mechanics and Physics of Solids* 34: 293-304.

[3]At $800°C$ for one hour in an inert atmosphere. This heat treatment yields a reasonably random distribution of grain orientations.

[4]All data from experimental pole figure measurements was processed using the *popLA* computer program by Kallend *et al.* (1989).

[5]The procedure for determining the material parameters appearing in the viscoplastic part of the constitutive functions have been detailed by these authors in their recent paper.

Asaro, R. J., and Needleman, A., 1985. Texture Development & Strain Hardening in Rate Dependent Polycrystals. *Acta Metallurgica* 33: 923-953.

Brown, S. B., Kim, K.H., & Anand, L. , 1989. An Internal Variable Constitutive Model for Hot Working of Metals. *International Journal of Plasticity* 5: 95-130.

Hill, R., 1967. On the Classical Constitutive Relations for Elastic/Plastic Solids. *Recent Progress In Applied Mechanics. The Folke-Odqvist Volume*, Wiley, New York, pp. 241-249.

Hughes, T. J. R., 1984. Numerical Implementation of Constitutive Models: Rate Independent Deviatoric Plasticity. *Theoretical Foundation for Large-Scale Computations of Nonlinear Material Behavior*, Nemat-Nasser S., Asaro, R. J., and Hegemier, G. A., eds., Martinus Nijhoff Publishers, Boston, pp. 29-57.

Kalidindi, S. R., Bronkhorst, C. A., & Anand, L., 1992. Crystallographic Texture Evolution in Bulk Deformation Processing of FCC Metals. *Journal of the Mechanics and Physics of Solids* 40: 537-569.

Kallend, J. S., Kocks, U. F., Rollett, A. D., & Wenk, H. R., 1989. *popLA: The Preferred Orientation Package from Los Alamos*, Los Alamos.

Lush, A. M., Weber, G., & Anand, L., 1989. An Implicit Time-Integration Procedure for a Set of Internal Variable Constitutive Equations for Isotropic Elasto-Viscoplasticity. *International Journal of Plasticity* 5: 521-549.

Molinari, A., Canova, G. R., & Ahzi, S., 1987. A Self-Consistent Approach of the Large Deformation Polycrystal Viscoplasticity. *Acta Metallurgica* 35: 2983-2994.

Taylor, G. I., 1938. Plastic Strain in Metals. *Journal of the Institute of Metals* 62: 307-324.

Weber, G., & Anand, L., 1990. Finite Deformation Constitutive Equations and a Time Integration Procedure for Isotropic, Hyperelastic-Viscoplastic Solids. *Computer Methods in Applied Mechanics and Engineering* 79: 173-202.

MECAMAT'91, Teodosiu, Raphanel & Sidoroff (eds) © 1993 Balkema, Rotterdam, ISBN 90 5410 317 5

Modelling of the induced anisotropy in inelastic bodies

Angel I. Baltov
Institute of Mechanics and Biomechanics, Sofia, Bulgaria

ABSTRACT: Processes of oriented plastic deformation and damage which induce an anisotropy of the inelastic properties are analysed in the paper. The model parameters are determined by performing a combination of one-dimensional experiments and by employing a microimitation approach (a combination between the experimental technique of speckle interferometry and FEM).

1 INTRODUCTION

We take into account metal forming processes with large plastic deformations. The orientation of the external loading due to metal forming leads to the orientation of the plastic deformations as well. This causes the development of material plastic anisotropic hardening. This problem has been studied for many years and a number of papers throw light upon the experimental study and the mathematical modelling of the phenomena (see for example Baltov 1990, Szczepinski et al. 1971, etc.). Recently, systematic studies have been performed to clarify the effect of induced plastic anisotropy on the formation of plastic localization bands, on the initiation and development of damage and macrofracture, etc. (Duszek-Perzyna 1988, Baltov et al. 1989, etc.). The damage (i.e. initiation and growth of: (1) bands of localization of plastic microstrains in crystal grains; (2) shear and spallation microcracks within grains and intergranular zones; (3) microvoids, etc.) is generally oriented in accordance with the external loading. This orientation causes the anisotropy of the inelastic properties. The joint effect of the oriented plastic deformation and damage is an object of study of many papers (Cordebois and Sidoroff 1982, Lemaitre and Chaboche 1985, Murakami 1983, Dacheva 1989, etc.). The problem is treated by an appropriate introduction of tensor and vector measures of damage and by the definition of appropriate limit surfaces in the stress space where these measures take place. The basic difficulty during modelling of the studied phenomena is the restricted number of experimental results. A difficult experimental problem is to separate the effects of plastic strain and damage on the induced anisotropy of the material inelastic properties. A confirmed approach to estimate this effect is the so-called microimitation approach (Litewska et al. 1984). According to it, an infinitesimal neighbourhood of a body point is imitated by a finite region of the same material, where there are artificially created defects (cracks, voids, etc.), controlled by the experimentalist. This approach is applied in the present paper in order to develop a method for the description of the induced anisotropy. The method combines speckle interferometry experiments and FEM calculations.

We propose a new model, describing more completely the induced anisotropy due to the oriented plastic deformation and damage. The necessity to describe the effects of induced anisotropy is related to the development of systems for automated design of technological processes where models, simulating real processes, are essentially used. The account of his anisotropy is very important for multistage metal forming processes.

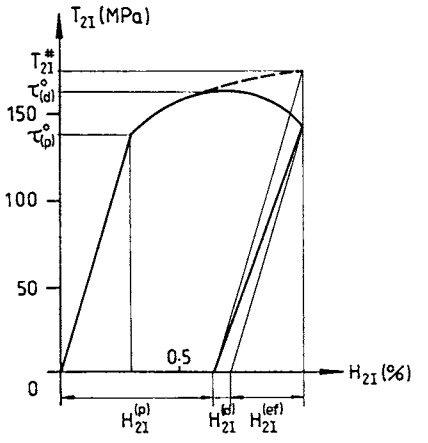

Fig. 1 Nominal stress - nominal strain curve for pure aluminium thin-walled specimen deformed in torsion

2 A MODEL DESCRIBING THE INDUCED ANISOTROPY DUE TO PLASTIC DEFORMATION AND DAMAGE

We consider quasistatic deformation of metallic bodies with crystal microstructure: crystal grains and intergranular zones. Plastic deformation and damage (over a definite level of plastic strain) develop during metal forming. They cause microstructural changes which induce an anisotropy of the inelastic properties. During plastic deformation, microstrain localization bands occur in the crystal grains, which are oriented in accordance with the external loading and the generated slip lines. This causes the anisotropy of the plastic properties on a macroscopic level. The shear microstresses within the bands can reach the material shear strength when the external loading increases, and consequently shear microcracks can occur. The latter have the same orientation as the localization bands. However, this can change the deformation anisotropy on a macroscopic level but does not affect its character. For larger external loads, microdefects of other character may develop: (1) microcracks due to shear between the grains; (2) microcracks due to spallation within the grains and in the intergranular zones; (3) microvoids due to grain intermixing, separation from inclusions, etc. These defects induce also a macroscopic anisotropy because of their oriented character. On the macroscopic level, the material displays different behaviours in tension and compression (the microcracks close under compression, etc.).

Our macroscopic model is based on assumptions, prompted by the analysis of experimental evidence. In order to consider more directly the experimental process of plastic deformation involving large strains, a mixed description is proposed (Baltov 1985). We introduce the material coordinate system OX_J, (J = I, II, III) and the space coordinate system Ox_i, (i = 1, 2, 3), as well as the mixed process measures: the first Piola-Kirchhoff stress tensor T_{iJ} and the displacement gradient H_{iJ}. A relation between the components T_{2I} and H_{2I} for technically pure aluminium is given in Figure 1. This relation is obtained from experiments on torsion of thin-walled tubular specimens, under the assumption of a uniform distribution of the shear stress over the tube wall (Baltov and Yankov 1989). Up to a stress level $\tau^{o}_{(p)}$, the material deforms elastically, then elasto-plastically between $\tau^{o}_{(p)}$ and $\tau^{o}_{(d)}$, while over $\gamma^{o}_{(d)}$ the damage process is initiated (see Figures 1 and 2). Due to damage, unloading proceeds with a changed elastic modulus. This allows to define a residual plastic strain $H^{(p)}_{2I}$, a fictitious elastic strain $H^{(ef)}_{2I}$ related to the elastic modulus of the undamaged material and a strain due to damage - $H^{(d)}_{2I}$. The damage description by means of deformation measures is an approach often used in literature (Ilyushin 1967, Dragon and Mróz 1979, Baltov (1981).

The model linearization of the relation T_{2I}-H_{2I} is given in Figure 2. It allows to derive some simplified but useful relations. Let $H^{(ef)}_{2I} = H_{2I} - (H^{(p)}_{2I} + H^{(d)}_{2I})$; μ_o is the initial shear modulus of the undamaged material; $\mu_{(p)}$ is the tangential modulus of plastic strain; $\mu_{(d)}$ is the tangential modulus of damage with plastic deformation; μ is the elastic modulus of the damaged material. We obtain the following relations

$$T_{2I} = 2\mu_o H^{(ef)}_{2I} = 2\mu(H^{(ef)}_{2I} + H^{(d)}_{2I}), \qquad (1)$$

$$T_{2I}^{\#} = 2\mu_o\left(H_{2I}^{(d)} + H_{2I}^{(ef)}\right), \qquad (2)$$

$$T_{2I}^{\#} - T_{2I} = 2\mu_{(p)}\left(H_{2I} - \frac{(\tau_{(d)}^{o} - \tau_{(p)}^{o})}{2\mu_{(p)}} - \frac{\tau_{(p)}^{o}}{2\mu_o}\right) \qquad (3)$$

$$T_{2I}^{\#} - T_{2I} = 2\mu_o H_{2I}^{(d)} \qquad (4)$$

where $T_{2I}^{\#}$ is a fictitious stress given in Figure 2.

A lot of experiments exist, demonstrating plastic and damage induced anisotropy (see e.g. Cordebois and Sidoroff 1982, Litewka et al. 1984, Wu et al. 1990. An exemple is given in Figure 4. The figure shows the relation between the mean stress P and the volume change V, presenting the Bauschinger effect (Wu et al. 1990). $V^{(d)}$ denotes the residual volume change.

On the basis of these and other experimental studies, we make the following assumptions.

The process measures are given in a mixed description by introducing two coordinate systems; a material rectangular coordinate system (OX_K, K = I, II, III) and a spatial rectangular coordinate system (Ox_i, i = 1, 2, 3).

a) For the stress state : the first Piola-Kirchhoff stress tensor, i.e. $T_{iK}(X_M,t)$, $X_M \subset \Omega_o$, $t \in [t_o,t_1]$, where Ω_o is the region occupied by the body at the initial time t_o, while t_1 indicates the time at which the process under consideration ends; the deviator stress is designated by S_{iK}, and the mean stress by

$$P = \frac{1}{3}\delta_{jM}T_{jM},$$

δ_{jM} being a unit tensor of transition between the two coordinate systems. To obtain a unified form for the yield condition, we use the following expression: $T_{iK} = S_{iK} + eP\delta_{iK}$, where e is equal to 1 when the residual volume change is taken into account, and equal to 0 in the opposite case. For a significant nucleation of microvoids, T_{iK} is replaced by the equivalent stress $T_{iK} = S_{iK} + e(V^{(d)})\delta_{iK}P$, where the function $e(V^{(d)})$ is determined experimentally.

For the stress rate: $\dot{T}_{iK} = \frac{\partial T_{iK}}{\partial t} - \Omega_{ij}T_{jK}$, with $\Omega_{ij} = \frac{1}{2}\left(\delta_{iK}T_{jK} + \delta_{jK}T_{iK}\right)$.

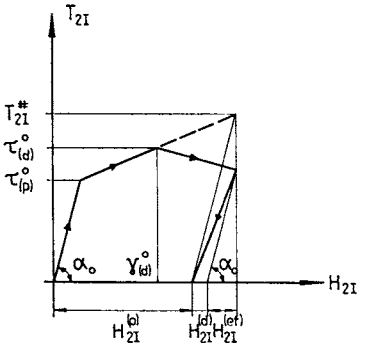

Fig. 2 Proposed linearization of the stress - strain curve shown in Figure 1.

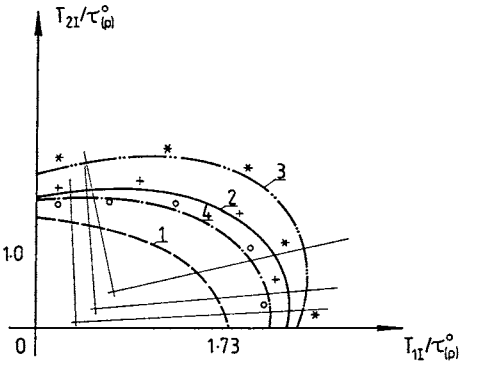

Fig. 3. Subsequent yield ellipses ($\gamma^{(p)} = 0.05$) for aluminium alloy (μ_o = 26 GPa, b=0.12, A=-7×10^{-2} m^4/N^2, K=42.1, c=380 MPa, c_o=220 MPa).

1 - Initial von Mises yield ellipse
2 - Yield ellipse for $Y_o^{(d)} = 0.20$, α=30°
3 - Yield ellipse for $Y_o^{(d)} = 0.20$, α=50°
4 - Yield ellipse for $Y_o^{(d)} = 0.30$, α=30°

For the stress rate: $\dot{T}_{iK} = \frac{\partial T_{iK}}{\partial t} - \Omega_{ij}T_{jK}$, with $\Omega_{ij} = \frac{1}{2}\left(\delta_{iK}T_{jK} + \delta_{jK}T_{iK}\right)$.

b) For the strain state: the displacement gradient $H_{iK}=U_{i,K}$, where $U_i(X_M,t)$ is the displacement vector and the comma denotes the differentiation with respect to X_K; the material strain tensor E_{KL} is then equal to

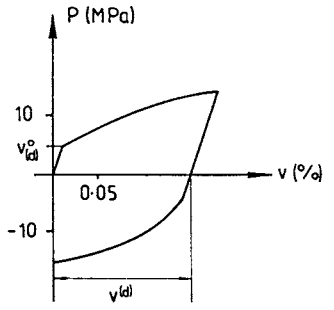

Fig. 4 Hydrostatic stress - strain curve

$\frac{1}{2}(\delta_{iK}H_{iL} + \delta_{iL}H_{iK} + H_{iK}H_{iL})$; the rate of the displacement gradient is designated by: $V_{iK} = \dot{H}_{iK}$.

c) For the plastic deformation: the plastic part of the displacement gradient $H_{iK}^{(p)}$; the intensity by $\gamma^{(p)} = \sqrt{\frac{1}{2}\tilde{H}_{iK}^{(p)}\tilde{H}_{iK}^{(p)}}$, with $\tilde{H}_{iK}^{(p)} = H_{iK}^{(p)} - \frac{1}{3}\delta_{iK}\delta_{jM}H_{jM}^{(p)}$; its rate $V_{iK}^{(p)}$.

d) For the damage: the part of the displacement gradient due to microfracture $H_{iK}^{(d)}$, its intensity $\gamma^{(d)} = \sqrt{\frac{1}{2}\tilde{H}_{iK}^{(d)}\tilde{H}_{iK}^{(d)}}$, with $\tilde{H}_{iK}^{(d)} = H_{jK}^{(d)} - \frac{1}{3}\delta_{iK}\delta_{jM}H_{jM}^{(d)}$; its rate $V_{iK}^{(d)}$.

e) For the microstructural changes, the following stress tensors are used:

(1) a microstress tensor due to the plastic deformation $T_{iK}^{(p)}$, its deviatoric part $S_{iK}^{(p)}$ and $T_{iK}^{(p)} = S_{iK}^{(p)} + \frac{1}{3}e_o\delta_{iK}\delta_{jM}T_{jM}^{(p)}$, where e_o is equal to 1 when the oriented nucleation of microvoids is considered and equal to 0 in the opposite case.

(2) a microstress tensor due to damage $T_{iK}^{(d)}$, its deviatoric part $S_{iK}^{(d)}$ with $T_{iK}^{(d)} = S_{iK}^{(d)} + \frac{1}{3}e_o\delta_{iK}\delta_{jM}T_{jM}^{(d)}$. We introduce also an internal state variable $Y_{iK}^{(d)} = -\frac{1}{b}T_{iK}^{(d)}$, linearly related to $T_{iK}^{(d)}$, where b = const. is experimentaly obtained.

The model assumptions are:

a) The displacement gradient H_{iK} consists of a fictitious elastic part $H_{iK}^{(ef)}$, corresponding to the elastic characteristics of the undamaged material, a plastic part $H_{iK}^{(p)}$, and a part due to damage $H_{iK}^{(d)}$, i.e.

$$H_{iK} = H_{iK}^{(ef)} + H_{iK}^{(p)} + H_{iK}^{(d)} \tag{5}$$

or in terms of rates

$$V_{iK} = V_{iK}^{(ef)} + V_{iK}^{(p)} + V_{iK}^{(d)} \tag{6}$$

b) The rate of the elastic part $V_{iK}^{(ef)}$ is related to the stress rate $\dot{T}_{iK}$ through Hooke's law (the elastic deformations are small):

$$V_{iK}^{(ef)} = H_{iKjL}\dot{T}_{jL} \tag{7}$$

where H_{iKjL} is the tensor of elastic resistance for undamaged materials.

c) The rate of the plastic part $V_{iK}^{(p)}$ is expressed by means of the flow rule, associated with the yield condition F = 0.

$$V_{iK}^{(p)} = -\dot{\Lambda}\frac{\partial F}{\partial T_{iK}^{(p)}},$$

$$\dot{\Lambda}\begin{cases} = 0, \text{if } F < 0 \text{ or } F = 0, \text{but } L \le 0 \\ > 0, \text{if } F = 0 \text{ and } L > 0 \end{cases} \tag{8}$$

where $L = \frac{\partial F}{\partial T_{iK}}\dot{T}_{iK}$

The tensors $H_{iK}^{(p)}$ and $T_{iK}^{(p)}$ are thermodynamically coupled and $T_{iK}^{(p)}$ is the internal

$$V_{iK}^{(d)} = \dot{\Lambda}\frac{\partial F}{\partial Y_{iK}^{(d)}} = -\bar{b}\,\dot{\Lambda}\frac{\partial F}{\partial T_{iK}^{(d)}}, \tag{9}$$

where

$$T_{iK}^{(d)} = -\bar{b}\,Y_{iK}^{(d)},$$

$$\bar{b} = \begin{cases} 0, & \text{if } \gamma^{(d)} \le \gamma_{(d)}^{o} \quad \text{or } P \le 0 \\ b, & \text{if } \gamma^{(d)} > \gamma_{(d)}^{o} \quad \text{and } P > 0 \end{cases} \tag{10}$$

where $P = \frac{1}{3}\delta_{jM}T_{jM}$

$H_{iK}^{(d)}$ and $T_{iK}^{(d)}$ are thermodynamically coupled and $T_{iK}^{(d)}$ is the internal state variable.

e) The yield condition has the form

$$F \equiv \frac{3}{2} N_{iKjL} \overline{T}_{iK} \overline{T}_{jL} - \sigma^2 = 0, \qquad (11)$$

where

$$N_{iKjL} = \frac{1}{2}(\delta_{iK}\delta_{jL} + \delta_{jK}\delta_{iL}) + A T_{iK}^{(a)} T_{jL}^{(a)},$$

$$\overline{T}_{iK} = T_{iK} - T_{iK}^{(a)}$$

$$T_{iK}^{(a)} = T_{iK}^{(p)} - T_{iK}^{(d)} \qquad (12)$$

$$\sigma = \sqrt{3}\,\tau \;,\; \tau = \tau_{(p)}^{o}(1 + K\gamma^{(p)})\left(1 - \frac{\gamma^{(d)}}{\gamma^*}\right).$$

In these equations, the parameter A describes the anisotropic hardening (Baltov and Sawczuk 1965) and K is the isotropic hardening coefficient. The parameter γ^* is the limit value of the strain intensity due to damage and is taken as constant. When the strain reaches this value, macrofracture begins. It is interesting to note that a full tensor in the yield condition has been used by Arutunyan and Markov (1977) for the case of plastic dilatation. If we assume that $e = e(V^{(d)})$ and $A \equiv 0$, and the so-obtained yield conditions are similar to those of Duszek and Perzyna (1988). $\overline{T}_{iK}$ is the tensor of active stresses, and $T_{iK}^{(a)}$, that of inelastic stresses (Baltov and Boncheva 1982). The yield condition describes the anisotropy induced by the plastic deformation and damage. When damage is only due to shear microcracks along localization bands, condition (12) is modified into an expression containing the stress deviators i.e., since $e = 0$, $e_o = 0$, $\overline{S}_{iK} = S_{iK} - S_{iK}^{(a)}$, $S_{iK}^{(a)} = S_{iK}^{(p)} - S_{iK}^{(d)}$. In this case, the volume change V has not reached the limit marking the start of microvoid formation $V_{(d)}^{o}$. We consider the material to be rate-in sensitive during the analysed quasi-static process. We assume that the process is isothermal (θ = const) and do not take into account heat sources due to energy dissipation during the inelastic deformation. We consider a linear model where A, b, K, etc. are material constants. In the general case, τ and A will be nonlinear functions of the process parameters ($\gamma^{(p)}$, $\gamma^{(d)}$, $V^{(d)}$, θ) (Baltov 1990).

f) The equation of the evolution of the internal state variables $T_{iK}^{(p)}$ and $T_{iK}^{(d)}$ are assumed to be linear

$$\dot{T}_{iK}^{(p)} = c\; V_{iK}^{(p)} \text{ and } \dot{T}_{iK}^{(d)} = c_o V_{iK}^{(d)} \qquad (13)$$

where c and c_o are material constants, characterizing the induced anisotropy.

The following relations follow from our assumptions:

a) The relation between the rates of displacement gradients for inelastic deformation is:

$$V_{iK}^{(d)} = \overline{b}\; V_{iK}^{(p)}. \qquad (14)$$

b) The flow rule has the following form:

$$V_{iK}^{(p)} = -\; \dot{\Lambda} F_{iK}^{(p)}, \qquad (15)$$

where

$$F_{iK}^{(p)} = \frac{\partial F}{\partial T_{iK}^{(p)}} = F_{iK} + 9\,\overline{P}\,A\,\Sigma_{(a)}\delta_{iK}$$

$$\overline{P} = \frac{1}{3}\delta_{jM}\overline{T}_{jM}\;,\; \Sigma_{(a)} = T_{jL}^{(a)}\;\overline{T}_{jL},$$

$$F_{iK} = \frac{\partial F}{\partial T_{iK}} = 3N_{iKjL}\overline{T}_{jL} = 9\overline{P}\delta_{iK} + 3A\,\Sigma_{(a)}\,T_{iK}^{(a)}, \qquad (16)$$

$$\dot{\Lambda} = \frac{1}{H_{(p)}}\;\frac{L}{2\sqrt{3}\,\sigma\,\tau_{(p)}^{o}}$$

$$H_{(p)} = \left|c\Sigma_{(f)}/(2\,\sigma\sqrt{3}\tau_{(p)}^{o}) - \frac{K}{2\gamma^{(p)}}\left(1 - \frac{\gamma^{(d)}}{\gamma^*}\right)\Sigma_{(p)} + \frac{\overline{b}\,(1+K\gamma^{(p)})}{2\,\gamma^{(d)}\,\gamma^*}\,\Sigma_{(d)}\right|^{-1},$$

$$\Sigma_{(f)} = F_{iK}^{(p)}\;F_{iK}^{(p)},\quad L = F_{iK}\;\dot{T}_{iK},$$

$$\Sigma_{(p)} = H_{iK}^{(p)}\;F_{iK}^{(p)},\; \Sigma_{(d)} = H_{iK}^{(d)}\;F_{iK}^{(p)}.$$

We discuss the problem of the model parameters identification in the next paragraph.

3 MICROIMITATION APPROACH, IDENTIFICATION OF THE MODEL PARAMETERS

The determination of the model parameters can be done on the basis of a combined system of experiments. In general these must be:

a) One-dimensional experiments of tension or torsion of thin-walled tubular specimens. The following parameters are thus determined: $\tau^o_{(p)}$, $\tau^o_{(d)}$, μ_o, $\mu_{(p)}$, $\mu_{(d)}$, μ, and γ^*.

b) Experiments characterized by a mean stress $\overline{P}$ and a volume change V and where the residual volume change $V^{(d)}$ is recorded and the volume elastic modulus of the undamaged material K_o, the start of the microvoid nucleation which leads to the occurrence of a residual volume change $V^o_{(d)}$, etc. are determined.

c) Two-dimensional experiments for the determination of the parameters A, c, c_o, K. These can be classical experiments with thin-walled tubular specimens, tension of plates and cutting of specimens at different angle with respect to the plate axis, cross-like specimens, etc. It is difficult to estimate the degree of damage by performing these experiments. Hence, we recommend the microimitation approach (Litewska et al. 1984).

We apply the microimitation approach to the testing of a flat rectangular specimen (l_I x l_I x δ, $\delta << l_I$, l_I is the initial dimension of the specimen and δ is its thickness) which is tested under plane stress. This specimen imitates an infinitesimal neighbourhood of a material point. We shall discuss the special case of damage due to shear cracks. Cracks are formed in the specimen under different α angles with respect to the specimen axis, so that a given damage degree $Y_o^{(d)}$ can be attained. However,

$$Y_o^{(d)} = n\, m\, \frac{a_o}{L_o(\alpha)},$$

where n is the number of cracks, with length a_o; m is a number of lines with cracks and $L_o(\alpha)$ is the average length of a line at angle α in the specimen. Along the boundaries of the flat specimen, small displacement increments are applied until the prescribed values U_1 and U_2 are obtained.

We introduce two coordinate systems with coinciding axes (OZ_K, K = I, II, III) and (Oz_i, i = 1, 2, 3). We apply three systems of displacements:

$$(1)\quad U_1(Z_I) = \sum_{\xi=1}^{n+1} \Delta U_{1(\xi)}(Z_I)\,,$$

$$U_2(Z_I) = \sum_{\xi=1}^{n+1} \Delta U_{2(\xi)}(Z_I)\,;$$

$$(2)\quad U_1(Z_{II}) = \sum_{\xi=1}^{n} \Delta U_{1(\xi)}(Z_{II})\,,$$

$$U_2(Z_{II}) = \sum_{\xi=1}^{n+1} \Delta U_{2(\xi)}(Z_{II})\,;$$

(3) a combination between (1) and (2).

For each displacement increment $\Delta U_{1(\xi)}$ and $\Delta U_{2(\xi)}$, (ξ = 1, 2, ...,n + 1) the plane problem for an elastoplastic body with damage is solved by using the FEM. We obtain as a result the change of stresses $\Delta t_{iK(\xi)}$ and that of the displacement gradients $\Delta h_{iK(\xi)}$, $\Delta h^{(p)}_{iK(\xi)}$ in a grid of points within a region of the body. The formulation of the problem shows that the elastic and plastic characteristics are the same at "micro" and "macro" levels. The constitutive relations on the "micro" level are:

a) Yield condition:

$$F^* \equiv \frac{1}{2} n_{iKjL}\, \bar{s}_{iK} \bar{s}_{jL} - \tau^{*2} = 0, \qquad (17)$$

where

$$\bar{s}_{iK} = s_{iK} - s^{(p)}_{iK}\,,$$

$$s_{iK} = t_{iK} - \frac{1}{3}\delta_{iK}\,\delta_{jL} t_{jL},$$

$$n_{iKjL} = \frac{1}{2}\,(\delta_{iK}\,\delta_{jL} + \delta_{jL}\,\delta_{iK}) + A_o\, s^{(p)}_{iK}\, s^{(p)}_{jL}, \qquad (18)$$

$$\tau^* = \tau^o_{(p)} \left(1 + K_o \gamma^{(p)}_o\right),$$

$$\gamma_o^{(p)} = \sqrt{\frac{1}{2}\tilde{h}_{iK}^{(p)}\tilde{h}_{iK}^{(p)}}.$$

b) Flow rule:

$$\Delta\tilde{h}_{iK(\xi)}^{(p)} = -\Delta\lambda \frac{\partial F^*}{\partial t_{iK}^{(p)}},$$

$$\Delta\lambda \begin{cases} = 0, & \text{if } F^* < 0 \quad \text{or } F^* = 0, \quad L^* \le 0 \\ > 0, & \text{if } F^* = 0 \quad \text{and } L^* > 0 \end{cases}$$

where

$$L^* = F_{iK}^* \Delta t_{iK(\xi)}, \quad F_{iK}^* = \frac{1}{2} n_{iKjL}\bar{s}_{jL} \qquad (19)$$

c) Evolution equation:

$$\Delta s_{iK(\xi)}^{(p)} = c_o \Delta\tilde{h}_{iK(\xi)}^{(p)} \qquad (20)$$

The undamaged specimen undergoes a system of displacements (1) along its boundaries. The displacements are calculated at points of a grid introduced on the specimen. Speckle interferometry is applied for this displacement system and displacements are measured at the grid points. The results from the calculations and measurements are compared and parameters A_o , K_o , c_o are determined by using Kalman's method of nonlinear filter (Courage et al. 1990).

The macroscopic measures are determined on the basis of their relation to the microscopic ones:

$$\Delta T_{jL(\xi)} = < \Delta t_{jL(\xi)} >$$

$$\Delta H_{iK(\xi)} = < \Delta h_{iK(\xi)} > \qquad (21)$$

where the averaging < > is performed along the plane region boundaries. The final values are obtained by a summation

$$T_{jK} = \sum_{\xi=1}^{n+1} \Delta T_{jK(\xi)}, \quad H_{iK} = \sum_{\xi=1}^{n+1} \Delta T_{jK(\xi)}.$$

Let A_{iKjL}^o be the localization matrix. It is determined for each step of loading from the definition:

$$\Delta t_{iK(\xi)} = A_{iKjL}^o \Delta T_{jL(\xi)},$$

$$(i, j = 1, 2, K, L = I, II, \ \xi = 1, ..., n+1) \quad (22)$$

The 15 components of the matrix A_{iKjL}^o are determined from 15 algebraic equations obtained from equation (22), the latter being applied to the three systems of loading. On such a basis the plastic part of the displacements gradient is determined:

$$\Delta H_{iK(\xi)}^{(p)} = \frac{1}{S}\int_S A_{iKjL}^o \Delta h_{jL(\xi)}^{(p)} dS,$$

$$(i, j = 1, 2 : K, L = I, II; \ \xi = 1, ..n+1) \quad (23)$$

where S is the region occupied by the specimen in the plane OZ_IZ_{II}.

The part of the damage displacement gradient $\Delta H_{iK(\xi)}^{(d)}$ is equal to $\Delta H_{iK(\xi)}^{(p)}$ and the damage stress tensor $\Delta T_{iK}^{(d)} = c_o \Delta H_{iK(\xi)}^{(d)}$. A system of boundary displacements $U_I^*(Z_I) = 0$, $U_2^*(Z_{II}) = 0$ is applied to the specimen and unloading is performed. The residual inelastic measures $H_{iK}^{(p)}$, $H_{iK}^{(d)}$, $T_{iK}^{(p)}$, $T_{iK}^{(d)}$ are then calculated. We apply to the same specimen a system of boundary displacements (1) for different ratios U_1/U_2 until attaining the intensity of the current plastic strain $\gamma^{(p)} \approx 0.1$ %. Yield points in the plane (T_{1I}, T_{2I}) are thus determined. The points are approximated by an ellipse, originating from the yield condition

$$F \equiv R\,\bar{T}_{1I}^2 + M\,\bar{T}_{2I}^2 + 2N\,\bar{T}_{1I}\,\bar{T}_{2I} - \sigma^2 = 0, \quad (24)$$

where:

$$R = 1 + \frac{2}{3} A \left(T_{1I}^{(a)}\right)^2,$$

$$M = 3\left[1 + 2A\left(T_{2I}^{(a)}\right)^2\right],$$

$$N = \frac{3}{2} A\, T_{1I}^{(a)} T_{2I}^{(a)}.$$

Thus the constants A, K, c and c_o are determined by using the Least Square Method.

We consider an example with an aluminium alloy. Ellipses in (T_{II}, T_{2I}) for a different damage degree and angles are given in Figure 3. The figure illustrates the damage effect on the induced anisotropy, presented by the change of the yield surface in the stress space.

4 CONCLUSIONS

The analysis made shows the applicability of the model, created to describe the induced anisotropy of the material inelastic properties during coupled processes of plastic deformation and damage. This model is successfully applied to determine the anisotropy developed after the first stage of a two-stage forging of rectangular metal blocks. It seems reasonable to develop a nonlinear version of the model in our future analysis.

The analysis presented here has been partially performed during the author's stay in LMS, Ecole Polytechnique, Palaiseau, France, in 1990. The author is mostly grateful to the LMS Directorate for the excellent research conditions which he has been provided with.

REFERENCES

Arutunyan V.A. & K.Z. Markov 1977. Vestnik MGU 7: 27-32 (Russian).

Baltov A., A. Sawczuk, 1965. A rule of anisotropic hardening: *Acta Mechanica* I: 81-92.

Baltov A. 1981. Modelling of inelastic deformation and microfracture processes in ductile materials. *Proc. 4th Congress Theor. Appl. Mech.*: 531-536. Sofia : BAS Publ. House.

Baltov A. & N. Boncheva, 1982. A rule of anisotropic hardening with taking into account preliminary and actual plastic deformation and strain rates. *Euromech-115 : Comp. mécanique des solides anisotropes*: 243-256. Grenoble, 1980. Paris.

Baltov A. 1985. New aspects on the anisotropic hardening rule. *CIZM - Symp.: Plasticity Today*: 503-513. Ed. A. Sawczuk and G. Bianchi. London : Elsevier.

Baltov A. & R. Yankov 1989. Damage in isotropically plastic deformable bodies. *Proc. 6th Congr. Theor. Appl. Mech.* 1:15-20. Sofia : BAS Publ. House (Russian).

Baltov A., N. Bontcheva & R. Yankov 1989. Influence of damage and preliminary plastic deformation on crack propagation. Future Trends on Strength of Metals: 369-378. Volume in honour of Professor P.S. Theocaris. Athens.

Baltov A. 1990. New trends in the theory of anisotropic hardening bodies. Inelastic Solids and Structures, A. Sawczuk Memorial Volume: 1-12. Ed. M. Kleiber and J.A. Koning. Swansea U.K.: Pineridge Press.

Cordebois J. & F. Sidoroff 1982. Endommagement anisotrope en élasticité et plasticité, *J. Mech. Theor. Appl.*: 45-60.

Courage W.M.G., P.J. Schreurs & J.D. Janssen, 1990. Estimation of mechanical parameter values of composites with the use of FE and system identification techniques. *Composites and Structures*. 34: 231-237.

Dacheva M. 1989. Ph. D. Thesis, Inst. of Mechanics, Moskva.

Dragon A. & Z. Mróz 1979. A continuum model for plastic-brittle behaviour of rock and concrete. *Int. J. Engng. Sci.* 17: 547-558.

Duszek M.K. & P. Perzyna 1988. Influence of kinematic hardening on plastic flow localization in damaged solids. *Arch. Mech.* 40: 595-609.

Ilyushin A.A. 1967. On a theory of long-life strength. *Mech. of Solids*: 2-35 (Russian).

Lemaitre J. & J.L. Chaboche, 1985. *Mécanique des matériaux solides*. Paris: Dunod.

Litewska A., A. Sawczuk & J. Stanislawska 1984. Simulation of oriented continuous damage evolution. *J. Méc. Théor. Appl.* 3: 675-688.

Murakami S. 1983. Notion of continuum damage mechanics and its application to anisotropic creep damage theory. *J. Engng. Mat. Technol.* 105: 99-105.

Szczepinski W., I. Miastkowski & K. Turski 1971. Badania podstawowych praw wzmocneinia metali. IPPT-PAN: Warszawa.

Wu C.H., P.T. Wang, W.F. Pan & Z.Y. Xu 1990. Cyclic stress-response of porous aluminium. *Int. J. Plasticity* 6: 207-230.

MECAMAT'91, Teodosiu, Raphanel & Sidoroff (eds) © 1993 Balkema, Rotterdam, ISBN 90 5410 317 5

Glide softening in alloys: A simulation

G.Canova & L.P.Kubin
CNRS-ONERA (OM), UMR 104 CNRS, Châtillon, France

Y.Bréchet
LTPCM-ENSEEG, St.Martin d'Hères, France

ABSTRACT: The mechanisms by which precipitate shearing or the destruction of short range order lead to glide softening and strain localization in alloys are recalled. These phenomena have been simulated using a 3 D (dislocation discretized dynamics) technique which has been recently developed. Lüders-like deformation is obtained in easy glide while the successive nucleation of deformation bands occurs in duplex glide.

1: INTRODUCTION

It is widely recognized that the connection between the microscopic and macroscopic aspects of crystal plasticity involves the understanding of collective dislocation effects and of the intrinsic length scales associated with dislocation patterning. In the absence of convincing theoretical approaches to these problems, simulation methods have been developed in the past few years. An application is presented here to the case of plastic instabilities occurring through glide softening phenomena in alloys.

Two important causes of microstructural softening, the shearing of small coherent precipitates and the destruction of short range order are presented in Section 2. In both of these cases, plastic instabilities occur through a feed-back process between the reduction of glide resistance produced by dislocation shearing and the increase of slip activity in the softened regions. As a result, deformation by glide becomes nonuniform and these spatial instabilitites may lead to a reduction of strain hardening, sometimes to plastic instabilities on the deformation curves. The results of a three dimensional simulation of these effects in a model copper-base alloy are reported and discussed in Section 3.

The three dimensional simulation used in the present work bridges the gap between the scale of individual dislocations, whose properties are incorporated as input quantities, and that of the single crystal whose mechanical properties are obtained at the output. A detailed account of the simulation method, of its basic rules and of their physical justifications is given by Kubin and coworkers (1991). For this reason, only a brief summary is given below. The additional rules developed in order to adapt the method to the problem of glide softening are presented in Section 3.

The notion of critical annihilation distance is at the basis of the three dimensional simulation. It is illustrated by fig. 1 in the case of fcc crystals. At low and moderate temperatures, i.e., in the absence of climb, edge dislocations cannot leave their glide planes. Thus, two edge dislocations of opposite sign gliding in two parallel slip planes tend to form a stable dipolar configuration despite their mutual attraction. If, however, the distance between the two slip planes is smaller than a critical value y_e, the interaction stresses may approach the theoretical limit of the cristal. A mechanical collapse of the dipolar configuration occurs and the two dislocations mutually annihilate.

y_e, the critical annihilation distance for edge dislocations, is in practice the closest approach distance of two parallel dislocations, whatever their character. This quantity serves as a natural elementary length scale for the

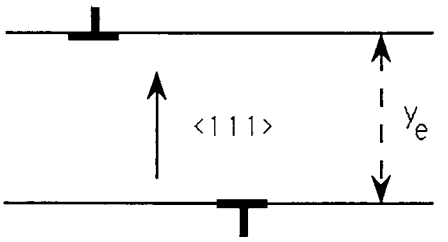

Fig. 1 The critical annihilation distance for edge dislocations, y_e, in the fcc lattice.

discretization of space in the simulation. In addition, its existence justifies the fact that there is an upper limit to the density of dislocations which can be stored in a deformed crystal. Essmann and Mughrabi (1979) have measured a value y_e = 1.5-1.6 nm in copper single crystals fatigued in the low amplitude saturation plateau.

Dislocation configurations are decomposed into sets of subsegments of edge or screw characters which are placed on a three dimensional fcc lattice. The lattice parameter, is such that the {111} interplanar spacing is consistent with the value of the critical annihilation distance. The three dimensional space is tiled with such elementary cells, building up a crystal of size $(10\ \mu m)^3$. From this starting point, the following properties are implemented quite naturally: the slip geometry, the long range elastic interactions between the various dislocation segments, the line tension of dislocations, the local effective stresses and dislocation free-flight velocities. Dislocation multiplication and direct annihilation as well as the formation of stable dipolar and multipolar structures occur, then, spontaneously within the simulation.

Additional rules are introduced to deal with dislocation intersections and cross-slip. The formation of sessile reaction products at the intersection of attractive, non coplanar, segments is the major mechanism contributing to strain hardening. Cross-slip processes play a double role: they allow mobile screw dislocations gliding in parallel slip planes to mutually annihilate. They also contribute to the relaxation of high local internal stresses and to the by-passing of localized obstacles by screw dislocations. Since cross-slip is a thermally activated phenomenon, a specification of the cross-slip parameters defines the simulated temperature. In adition, these parameters incorporate all the necessary information about the core structure i.e. they indirectly account for the value of the stacking fault energy of the material.

During one time step of the simulation each segments is moved once. The velocity of a dislocation segment moving between two forest obstacles in a perfect lattice is only limited by electron and phonon drag. With a typical mean-free path of 1 μm and a typical average free-flight velocity of 10 ms^{-1}, the time per step is of the order of 10^{-7} s. Within reasonable computing times it is possible to perform about 10^4 steps, yielding a strain of about one percent. Thus, the range of strain rates presently accessible to the simulation is around 10 s^{-1}. A total strain rate is imposed to the simulated crystal. The elastic properties of the ficticious testing system plus the specimen are characterized by an equivalent modulus ($M = 10^4$ MPa).

2: GLIDE SOFTENING IN ALLOYS

2.1 Glide Softening by precipitate shearing or destruction of short-range order

From a phenomenological point of view, plastic instabilitites can be classified into three main types according to the quantity which induces a decrease in the load carrying capacity of the specimen (Estrin and Kubin, 1991). This quantity can be the thermally activated component of the flow stress (thermomechanical effect), the strain rate hardening coefficient (i.e. strain rate softening) or the strain hardening coefficient (strain softening). Strain softening effects are very diverse (Luft, 1991). We consider here two types of glide softening mechanisms which are often encountered in Al or Cu based alloys, viz. the destruction of short range order (SRO) or of short-range segregation, and the shearing of small (typically 5 to 20 nm) coherent precipitates. Glide softening occurs through a feed-back process: the shearing of a slip plane by gliding dislocations reduces the local glide resistance by decreasing either the average precipitate radius or the degree of SRO in the solid solution. This induces slip localization as slip activity preferentially concentrates in slip zones where the glide resistance has partially

been destroyed, and further softens them.

In what follows, the component of the flow stress which can be destroyed by slip will be referred to, in a broad sense, as an alloy friction (τ_f). Once the alloy friction is reduced to zero or to its minimum value, strain hardening takes over in the cleared channels. Deformation further proceeds until the local glide resistance becomes equal to that of the virgin portions of the crystal. New slip zones are then initiated and this can occur by two mechanisms: the nucleation of fresh slip zones in other parts of the crystal or the expansion of the initial band in a Lüders-like manner. This last mechanisms is preferentially observed in crystals oriented for easy glide. In that case, the strain hardening rate is small, which allows for large strain concentrations

Whereas precipitate shearing has been recognized very early to be an effective strain softening mechanism, it took time to realize that the occurrence of planar slip in solid solutions is often due to the destruction of SRO and that it depends only weakly on the value of the stacking fault energy. This was established in particular through a careful study of the development of slip markings in single crystals of copper-base alloys (Neuhäuser, 1983; see also Olfe and Neuhäuser, 1988; Gerold and Karnthaler, 1989).

The problems which a simulation might attempt to solve are as follows: i) - what are the critical conditions defining the transition between Lüders-like propagation and the uncorrelated nucleation of slip bands ? ii) - What are the length scales involved, i.e., the band widths and velocities and, in particular, what is the origin of the observed fine structure of slip (Neuhäuser, 1983) ? iii) - What is the dislocation mechanism responsible for band propagation ? Classically, the propagation of Lüders bands is thought to occur either by cross-slip or through the activation of slip by long range stresses emitted at the moving front (Kocks, 1981). Another possible mechanism is the cooperative operation of two slip systems. iIV) - What are the consequences regarding the mechanical properties and the occurrence of macroscopic softening or of plastic instabilities ? In what follows, we discuss a first attempt to simulate glide softening processes. A systematic investigation where all the relevant physical parameters are varied is under way.

2.2. Softening by precipitate shearing

A softening rule is derived in the case of small, spherical, coherent precipitates. Similar arguments may apply to the destruction of SRO but, as discussed below, the situation is much more complicated in this last case.

The critical stress for overcoming shearable precipitates was derived by several authors (see Bréchet and Louchet, 1990):

$$\tau_c = \tau_0(R_0^{3/2}/\lambda b^{1/2}), \qquad (1)$$

where R_0 is the average radius of the intersection of the slip planes by precipitates, λ is the average precipitate spacing in the slip plane and b is the modulus of the Burgers vector. The constant stress τ_0 essentially depends on the line tension of the dislocations and on the energy of the planar fault (antiphase boundary) created by the shearing of a long range ordered precipitate. In many classical expressions, use is made in eq. (1) of the volume fraction of the precipitates, $f = (R_0/\lambda)^3$. In what follows and to avoid any confusion, the quantity R_0 refers to the initial radius of the precipitates or to dimensionlike coefficients which are conserved during straining, i.e., the average precipitate dimension perpendicular to the active slip plane, or an average dimension involved in the definition of the volume fraction. On the other hand, the length involved in eq. (1) is no longer R_0 under strain but an average radius, R, related to the sheared cross-section.

We now examine the relation between the local shear and the average precipitate radius in the slip plane, R. The {111} interplanar spacing of the lattice underlying the simulation (y_e = 1.6 nm) is in general smaller than the diameter of the precipitates ($2R_0 \approx$ 10 to 40 nm). Then, when n dislocations gliding in the same "plane" of the simulation have sheared the precipitate, the local shear is $\delta\gamma = nb/y_e$ (cf. figure 2). To determine the effective equivalent radius associated with the hatched area of fig. 2 b, we follow a simplified derivation given by Bréchet and Louchet (1990). The reduction in area is approximately equal to $-2nbR = -2y_eR\delta\gamma$, so that we can write:

$$2\pi R\delta R = -2y_eR\delta\gamma, \qquad (2)$$

and

$$\delta R = -(1/\pi) y_e \delta\gamma. \quad (3)$$

By integration, we obtain:

$$R = R_0(1 - \gamma/\gamma_0), \quad (4)$$

where $\gamma_0 = \pi R_0/y_e$ is the critical strain at which the effective radius vanishes. The result is approximate (indeed, $\gamma_0 = 2R_0/y_e$), but the definition of the equivalent radius necessarily involves some arbitraryness.

Combining eq. (1), where R_0 is replaced by R, and eq.(4), we eventually obtain

$$\delta\tau_c = -(3/2)\, \tau_{co}^{2/3} \tau_c^{1/3} (\delta\gamma/\gamma_0), \quad (5)$$

where τ_{co} is the initial value of the critical stress. This expression relates local shear increments to critical stress decrements. The microstructure is characterized by two mesoscopic quantities, γ_0 and τ_{co}. The value of τ_{co} is typically in the range 10 to 100 MPa, while γ_0 is simply the ratio of the precipitate diameter to y_e, e.g. $\gamma_0 \approx 6$ for $2R_0 \approx 10$ nm.

2.3. Softening by destruction of short-range order

In short-range ordered alloys, shearing involves the formation of a diffuse antiphase boundary whose configurational energy, W, can be estimated by examining the modifications of atom pair configurations below and above the slip plane (Pitsch, 1974; Büchner and Pitsch, 1985). This energy decreases with dislocation shearing, leading to a decreasing friction stress $\tau_f = W/b$. However, no general expression similar to eq. (5) can be derived in this case, as the configurational energies and their dependence on shearing depend much on the crystallographic structure of the alloy. Further, there can be local rearrangements of SRO through short-range diffusion and the friction stemming from SRO is not necessarily totally destroyed, even in the absence of diffusion.

In binary Al-Li alloys containing 2.5 wt.% Li, Bréchet (1987) estimates the maximum hardening due to SRO to about 6 MPa, while in Cu-12.6 at.% Zn, Olfe and Neuhäuser (1988) derive a value of about 10 MPa. The softening process is quite generally thought to be completed after the successive glide of a few dislocations, i.e., $\gamma_0 \approx 6b/y_e \approx 1$ for n = 6 dislocations.

Fig. 3 shows how deformation can spread out at atomic scale, leading to fine slip in a short-range ordered alloy, when several systems are simultaneously active. These cooperative slip processes are not presently introduced in the simulation but they deserve further discussion.

From this discussion we see that a precise description of the softening rules is not easy, even eq. (5) being approximate. In practice, the two important microstructural parameters are the initial strength and the critical strain. The detailed shape of the softening function probably does not matter much, provided it decreases monotonously.

3. NUMERICAL EXPERIMENTS

3.1. Conditions of the numerical experiments

Since the main objective of the present work is

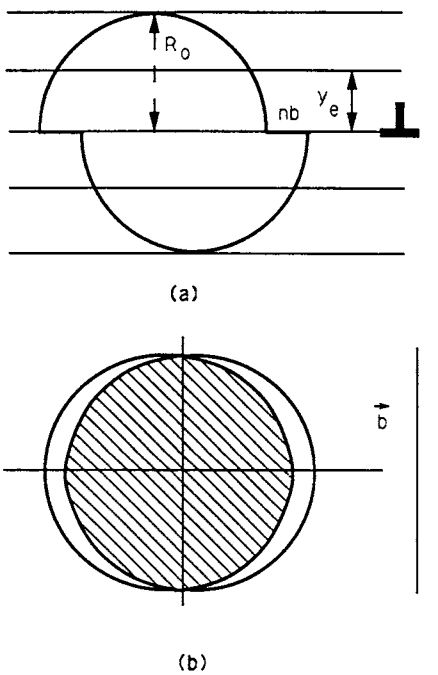

Fig. 2. A coherent precipitate (initial radius R_0) sheared by n dislocations of Burgers vector b, gliding in the same "slip plane" of the simulation. (a) - Side view. (b) - Top view.

to examine the spatial correlation of slip lines along a direction parallel to the specimen axis, some averaging procedure can be used to describe the distribution of the alloy friction in the slip planes. The alloy friction is, in what follows, assumed to be uniform in each {111} slip plane. Its value can, of course, vary along a direction parallel to the <111> normal. Therefore, individual events, like the shearing of a precipitate by a moving dislocation are not explicitely introduced. Doing this would, anyways, require a computing efficiency beyond reach in the present state of the simulation.

A convenient shape of the softening function has been defined, which contains both a critical strain and an alloy friction stress. For each slip plane of index i, counted along the <111> normal, we have

$$\delta\tau_{f,i} = - (\tau_{f,i} - \tau_p)\, \delta\gamma_i/\gamma_o, \qquad (6)$$

where $\delta\tau_{f,i}$ and $\delta\gamma_i$ are respectively the local alloy friction decrement and shear strain increment during one step of the simulation. $\tau_{f,i}$ is the current value of the alloy friction

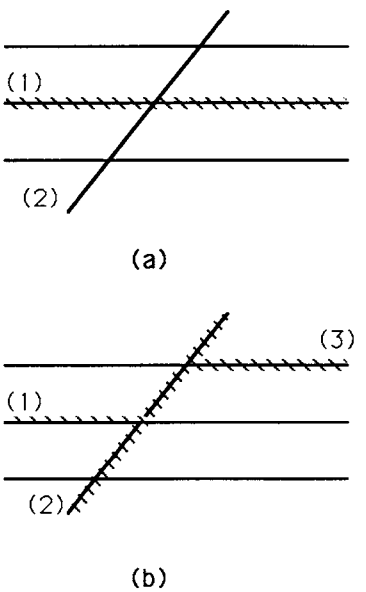

Fig. 2 The reduction of SRO by moving dislocations is represented by hatching. Successive activity in planes (1) and (2) and their mutual shearing favours the dispersion of SRO-destruction.

and τ_p is the intrinsic friction stress (the Peierls stress) of the material. The total number of slip planes is $i_{max} \approx 5800$ for each slip system. In copper, as in all fcc metals, the Peierls stress is very small and its value is $\tau_p \approx 3.10^{-5}\mu \approx 1.64$ MPa (μ is the shear modulus). A rather small value of γ_o was selected in order to obtain significant instabilities within a reasonable computing time: $\gamma_o = 0.2$. Finally, the initial value of the alloy friction was set to $\tau_{fo} = 6\ \tau_p \approx 10$ MPa. The shape of the averaged softening function, a decreasing exponential form, is somehow different from that derived in eq. (5) but, as already mentioned, this is not critical.

For the experiments reported here, two orientations were selected, [$\bar{1}$23] and [$\bar{1}$12], in order to achieve conditions of easy glide and duplex glide, respectively. The initial configuration (see Kubin and coworkers, 1991 for a discussion) is a random distribution of dislocation sources in total density $\rho_o = 10^{11}$ m^{-2} and of length $(\rho_i/2)^{-1/2} = 4.6$ μm. For the [$\bar{1}$23] orientation, all the segments have the same Burgers vector, [$\bar{1}$01]. When they have a screw character, the initial sources have two possible slip planes, (111) and (1$\bar{1}$1) but they are initially dissociated in one of them. To account for this, the glide system and the cross-slip system are selected at random with equal probabilities. For the [$\bar{1}$12] orientation, the initial density of sources is equally distributed into the two equivalent slip systems. The rule defined above for the selection of the preferred slip plane of the screw segments also applies in this case.

The other input parameters have been discussed in the Introduction. In particular, the simulated temperature is 300 K and the elastic constants as well as the cross-slip parameters are those of pure copper. This means, in practice, that cross-slip is difficult as long as the local internal stress opposing dislocation glide is smaller than 28 MPa, the critical stress for the onset of stage III on the deformation curve. Finally, the imposed total strain rate is 50 s^{-1} and the simulations were stopped when a total strain of about $5{\cdot}10^{-3}$ was reached.

3.2 Results

Figure 3 shows [$\bar{1}$01] views of the [$\bar{1}$23] crystal for increasing values of the average (total) strain. The active screw segments and the slip

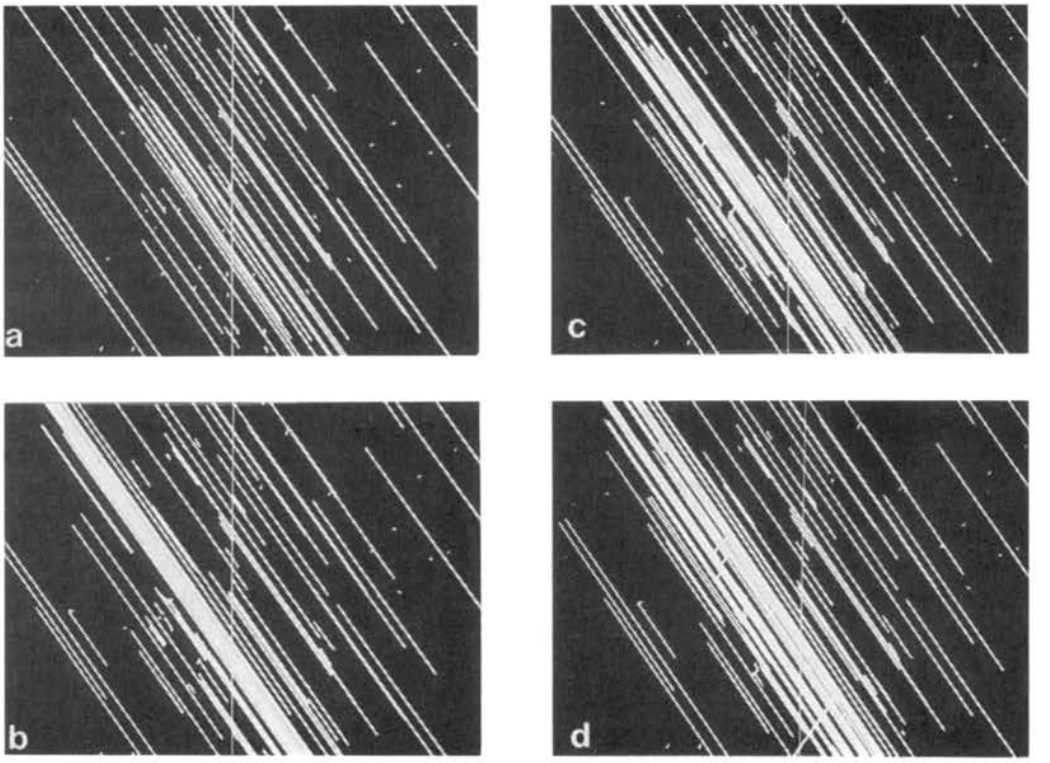

Fig. 3 [$\bar{1}01$] views of the [$\bar{1}23$] crystal deforming in easy glide for increasing values of the total strain. a: $\varepsilon = 10^{-3}$; b: $\varepsilon = 2.35 \cdot 10^{-3}$; c: $\varepsilon = 3.3 \cdot 10^{-3}$; d: $\varepsilon = 4.3 \cdot 10^{-3}$.

planes are perpendicular to the view plane and the edge segments are parallel to it, materializing the active slip lamellae. Slip localizes in one slip band which expands with increasing total strain. The fine structure of this band is clearly due to the initial distribution of the active sources, as will be seen more clearly below (cf. fig. 5). On figs. 3-c-d, the occurrence of edge segments oblique to the "slip traces" indicate that cross-slip and double cross-slip events have taken place.

Figure 4 shows the behaviour of the [$\bar{1}12$] simulated crystal which deforms in duplex glide. The viewing direction is parallel to [101], the direction common to the two active slip planes, ($\bar{1}11$) and ($11\bar{1}$). In this case, a different type of nonuniformity is obtained: several transient localizations occur successively on both of the active systems. This behaviour is associated with a strong interaction of the two slip systems, in particular with the formation of attractive junctions, as can be checked by looking at the same configurations from other points of view.

In each slip lamella, the Lüders strain can be defined as the strain at which the total glide resistance becomes identical to that of the undeformed material. This quantity is easily rationalized, at least qualitatively, in terms of the competition between softening and hardening. In duplex glide, the Lüders strain is necessarily smaller than in single glide, so that internal stresses in the active lamellae are not sufficient to induce propagation, either directly or through cross-slip mechanisms.

According to eq. (6), the local value of the alloy friction is a measure of the local shear. The alloy friction profiles of fig. 5 provide a simple way for examining the evolution of strain localization in the [$\bar{1}23$] crystal. In these

diagrams, the alloy friction $\tau_{f\,i}$ is plotted as a function of the position of the slip plane i along the <111> diagonal of the simulated crystal, for several values of the total strain. From the few sources which start operating at small strains (fig. 5-1), a small group develops in a cooperative manner (fig. 5-2) and concentrates all the slip activity. On fig. 5-2, the minimum value of the friction stress is close to 2 MPa and on fig. 5-3, the alloy friction is completely destroyed in several slip lamellae, the alloy friction having reached its minimum value of 1.64 MPa. In these regions the local strains are, therefore, larger than the characteristic value $\gamma_0 = 0.2$. A comparison of figs. 5-2, 5-3 and 5-4 shows that two processes occur in parallel, the expansion of the band by the nucleation of new, adjacent, slip lamellae and the progress of deformation inside the band.

At the largest strain (fig. 5-5) the slip band consists of a rather regular alternance of deformed and undeformed regions. In terms of the hierarchy of surface slip-steps defined by Neuhäuser (1983, cf. fig. 2), we have here a slip band subdivided into clusters of slip lines. The band width is 1.6 μm and the fine structure has a characteristic wavelength one order of magnitude smaller, of the order of 150 nm. This last length scale is usually thought to be determined by a critical distance associated with the cross-slip of screw dislocations (Nabarro, 1986). This is certainly the case here because the average distance between the initial sources is of the order of the micrometer. Therefore, only double cross-slip events could produce the fresh sources needed for the formation of the fine structure. Further, the critical annihilation distance for screw dislocations is y_s = 50-60 nm in copper at room temperature (Essmann and Mughrabi, 1979). This should lead, through annihilation mechanisms, to a pattern of wavelength $2y_s \approx$ 100-120 nm, consistent with the present numerical result.

The width of the regions where the alloy friction has totally been destroyed provides a measure of the band width w. This quantity is plotted on fig. 6 as a function of time. The thickness of the band increases linearly with time defining a constant propagation velocity v_b = 2.2 cm/s. According to Neuhäuser (1983), two types of Lüders band slip are observed in single crystals - those with the Lüders band front parallel to the primary slip plane ("G-bands"), like the one obtained here - those with the Lüders band front normal to the primary slip plane or "K-bands". For G-bands in neutron irradiated crystals, there is a linear relationship between the applied elongation rate, $\dot{e}$, and the band velocity v_b: $v_b/\dot{e} \approx 20$,

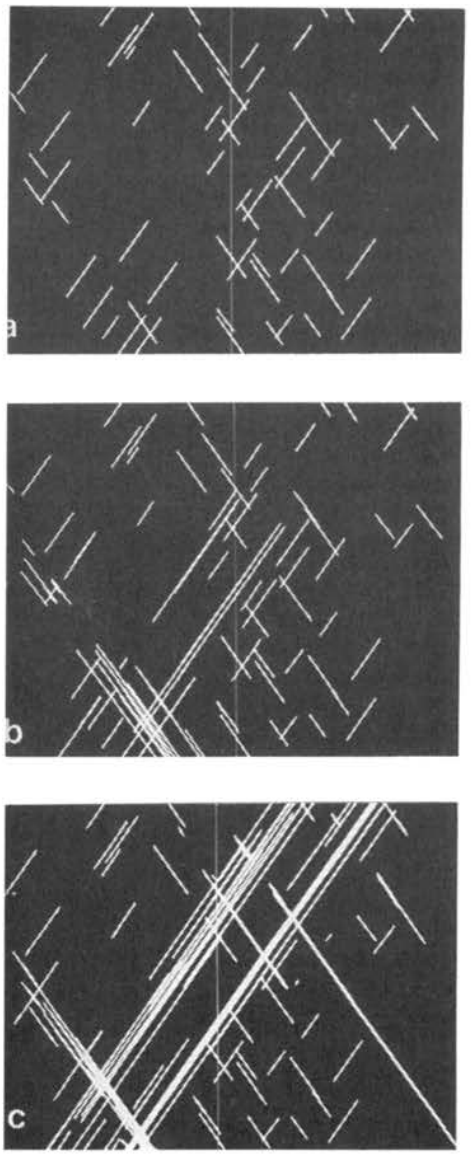

Fig. 4 [101] view of the [$\bar{1}$12] simulated crystal deforming in duplex glide. a: initial configuration, b: $\varepsilon = 10^{-3}$. c: $\varepsilon = 5.6 \cdot 10^{-3}$. Notice the occurrence of several slip bands.

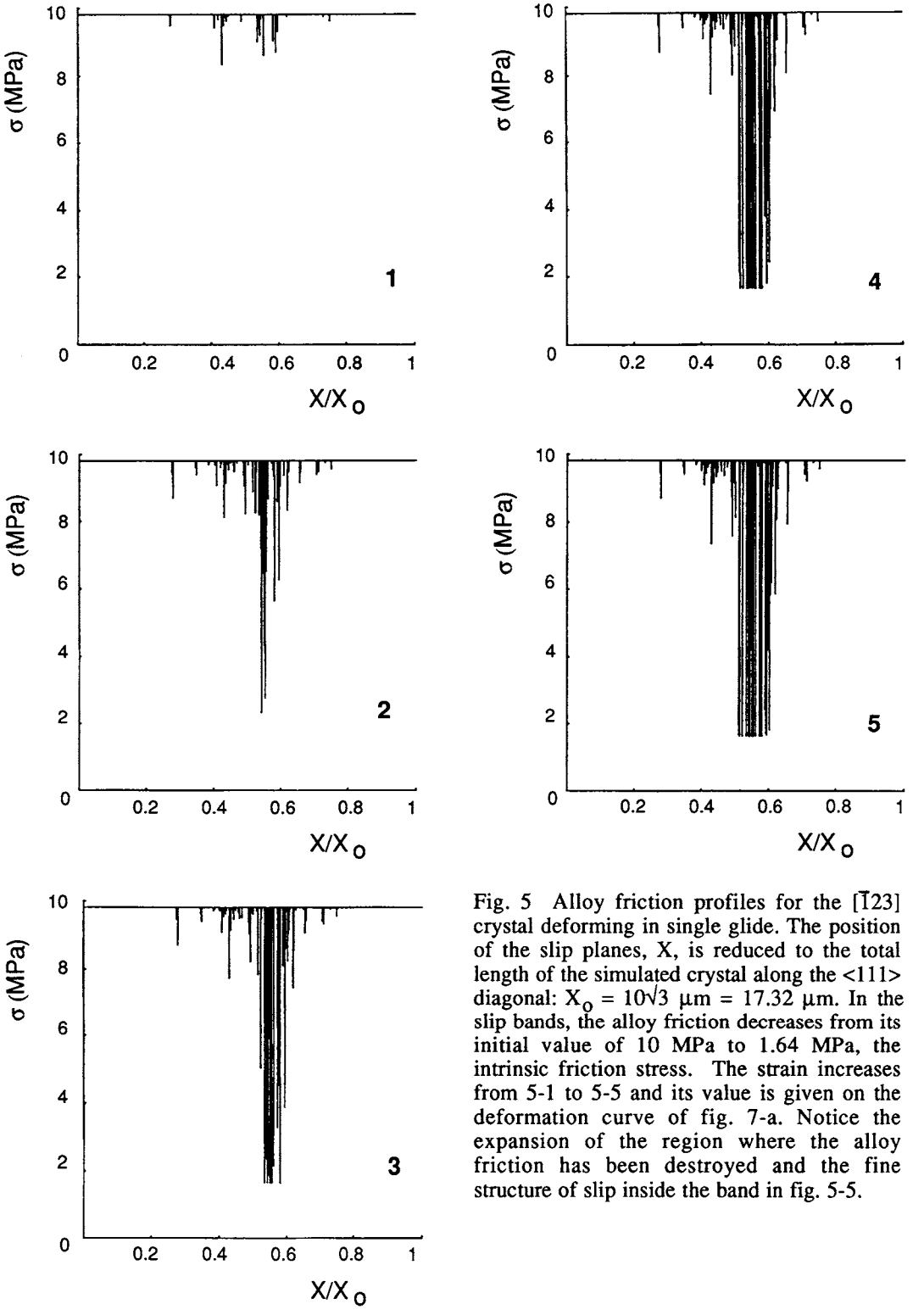

Fig. 5 Alloy friction profiles for the [$\bar{1}$23] crystal deforming in single glide. The position of the slip planes, X, is reduced to the total length of the simulated crystal along the <111> diagonal: $X_o = 10\sqrt{3}$ μm = 17.32 μm. In the slip bands, the alloy friction decreases from its initial value of 10 MPa to 1.64 MPa, the intrinsic friction stress. The strain increases from 5-1 to 5-5 and its value is given on the deformation curve of fig. 7-a. Notice the expansion of the region where the alloy friction has been destroyed and the fine structure of slip inside the band in fig. 5-5.

(Neuhaüser, 1988). In the present numerical experiment, the elongation rate is $\dot{e} = \dot{\varepsilon}_a l$, where $\dot{\varepsilon}_a = 50\ s^{-1}$ is the applied strain rate and $l = (14/9)^{1/2}.10^{-5}$ m is the length of the simulated crystal along the <123> direction. Hence $v_b/\dot{e} \approx 35$, a value comparable to that experimentally obtained in neutron irradiated crystals.

Figure 7 shows the stress-strain curves of the two simulated crystals. In both cases an early hardening stage is followed by macroscopic strain softening. As expected, the amplitude of the initial hardening stage is larger for the $[\bar{1}12]$ crystal. Given the time scale ($\delta t = \delta\varepsilon/\dot{\varepsilon} \approx$ 0.1 ms), the portions with negative strain hardening correspond to a rather abrupt yield drop. This behaviour is possibly due to the rather small value of the characteristic strain involved in eq. (6).

The shapes of these two deformation curves suggest that a steady state regime with a constant stress is about to be reached at the largest strain value. A stress plateau should correspond, at least in easy glide, to a band of active slip planes of constant width propagating with a constant velocity. The shape of the deformation curve of fig. 7-a can, then, be interpreted as follows. The band front has reached its steady state velocity (cf. fig. 6) while the strain rate profile behind the front is not yet in steady state.

The numbers on fig. 7-a refer to the alloy friction profiles of fig. 5. In particular, it is seen that the profile of fig. 5-2, which corresponds approximatively to the beginning of band propagation ($t = t_o$ on fig. 6) is obtained at the peak stress of the deformation curve.

4. DISCUSSION - CONCLUDING REMARKS

This numerical study illustrates the potentialities of the three dimensional simulation for understanding strain localization phenomena and band propagation effects in alloys. In the present stage, no definite conclusion can be drawn from these preliminary experiments and a systematic analysis of the dislocation configurations and of the influence of the parameters involved is being undertaken.

The list of the main physical parameters is as follows: two parameters are needed to describe the softening of the microstructure, the initial value of the friction stress and the characteristic strain associated with its decay. These two factors should influence the time scale of the yield drop, the band velocity, as well as the shape of the deformation curves. Other material parameters are those incorporated in the three dimensional simulation. Of principal interest here is the value of the cross-slip probability. The initial dislocation density and the orientation of the stress axis decisively influence the transition between successive nucleations and propagation by controlling the local strain hardening properties. Externally applied conditions involve the values of three quantities. - The temperature, which also governs the cross-slip probability. - The hardness of the simulated deformation setting. - The total strain rate or elongation rate.

It is important to notice that the quantity which scales the band velocity is not the applied strain rate but the elongation rate. As was shown by Neuhäuser (1983), there is a simple relationship between the Lüders strain ε_b or, equivalently, the extend of stage I, and the ratio $v_b/\dot{e}$:

$$v_b/\dot{e} = 1/\varepsilon_b \qquad (7)$$

The ratio of the elongation rate to the band velocity, as determined through the simulation, has a correct order of magnitude with a Lüders strain of the order of a few percent. This value is, of course, an average over the band whose deformation is nonuniform. Indeed it has been shown above that the local strains can be significantly larger than ε_b. In the results presented here, a steady state characterized by a deformation stage I has not been reached and the proportionality law of eq. (7) remains to be checked for various values of the applied elongation rate. However, the reasonable numerical agreement obtained so far seems to indicate that the essence of the propagation mechanism has been captured in the simulation. Other factors, like the specimen geometry, the influence of the bending moments due to the local shears in a specimen constrained at its extremities, the local reduction in cross-sectional area and the associated triaxiality of stress, may also influence the propagation velocity (Neuhäuser, 1983). Since these effects are not included in the simulation, they are

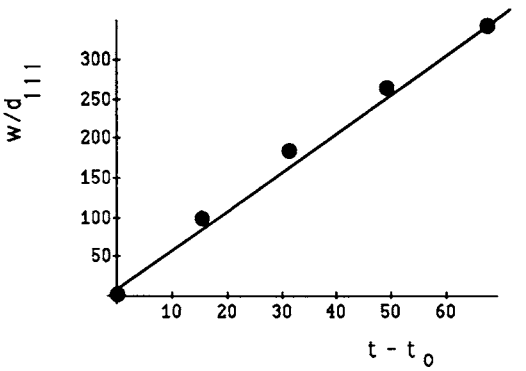

Fig. 6 [$\bar{1}$23] orientation. Time dependence of the band width w, reduced to the <111> interplanar spacing in the simulation. Time is reckoned from the moment t_0 where the alloy friction first reaches its minimum value in one slip plane.

probably not at the origin of the propagative behaviour and they should rather appear as correcting terms.

The Lüders strain being essentially a material property, propagation necessarily involves a dislocation mechanism, as already stressed by several authors (cf. Kocks, 1981). Further investigation of the output of the simulation at mesoscale is needed to trace back the events leading to the activation of slip at the front of the moving band. Although cross-slip and double cross-slip events are easily detected, one cannot rule out a priori the existence of dislocation pile-ups in the active regions and the related occurrence of long range stresses which may activate new dislocation sources. Thus, if cross-slip can be identified as the mechanism leading to the formation of the fine slip structure, there is as yet no certainty that it is responsible for band propagation. Two simple checks can be attempted to investigate how slip activity spreads out: i) set the cross-slip probability to zero and look at whether or not propagation still occurs. ii) Produce an intial configuration containing dislocation sources in a thin slice of the material and check if slip activity is able to propagate in the initially dislocation-free regions.

The occurrence of band propagation with a constant velocity leads to the possibility of phenomenological modelling in terms of reaction-diffusion forms. This has already been done for Lüders bands in polycrystals (Hähner, 1992). In such models, it is assumed that the dislocation mechanism responsible for propagation has a diffusive character. This reamins to be demonstrated in the case of the Lüders-like behaviour of single crystals. The transition between successive nucleations and propagation seems to involve local peaks of the internal stress rather than its average value. Whether or not this can be rationalized in terms of a diffusion-like mechanism remains to be investigated. Thus, a more thorough examination of the local dislocation microstructures and of the distribution of the internal stresses within the slip bands is worth being attempted. It could shed some light into the problem of the validity of reaction-diffusion forms.

Other interesting properties of the strain localizations are their evolution in time at a fixed position, the shape of their strain rate profiles and the value of the Lüders strains. The local strain hardening is made up of two additive contributions: the alloy softening, as given by eq. (5) or (6) and the dislocation strain hardening term, i.e., self-hardening in easy glide, forest hardening in multiple glide. A third contribution, presently not included in the simulation, stems from the local rotations associated with the local shears. Depending on the initial orientation of the crystal, this component may induce hardening or softening. For instance, in the case of the [$\bar{1}$23] crystal the Schmid factor is initially maximum and it decreases with increasing strain which induces a geometric hardening. This influence of this contribution on band properties, especially on the Lüders strain can be investigated as follows. In the present stage of the simulation, the lattice rotations are homogeneous inside the crystal, their value being defined through the average strains on each slip system. This can, however, be improved rather easily by inserting local rotations per slip plane, following a local rule analogous to that of eq. (6). Then, the local shear increment would determine the amount of both geometrical and alloying effects. The nonuniformity of the rotations inside the crystal may, in addition, induce elastic compatibility stresses and, possibly, plastic relaxations. For the moment it seems difficult to include these effects in the simulation.

At the macroscopic scale, several problems can be examined: the conditions of occurrence of strain softening, of yield points and of